

# Telemac3d

# Validation Manual

Otto Mattic

Version v7p3  
March 16, 2018



# Contents

<b>1</b>	<b>Cooper</b>	<b>11</b>
<b>1.1</b>	<b>Purpose</b>	<b>11</b>
<b>1.2</b>	<b>Description</b>	<b>11</b>
1.2.1	Reference .....	11
1.2.2	Geometry and Mesh .....	11
1.2.3	Physical parameters .....	11
1.2.4	Initial and Boundary Conditions .....	12
1.2.5	General parameters .....	12
1.2.6	Numerical parameters .....	12
1.2.7	Comments .....	12
<b>1.3</b>	<b>Results</b>	<b>12</b>
<b>1.4</b>	<b>Conclusion</b>	<b>12</b>
<b>2</b>	<b>NonLinearWave</b>	<b>13</b>
<b>2.1</b>	<b>Purpose</b>	<b>13</b>
<b>2.2</b>	<b>Description</b>	<b>13</b>
2.2.1	Reference .....	13
2.2.2	Geometry and Mesh .....	13
2.2.3	Physical parameters .....	14
2.2.4	Initial and Boundary Conditions .....	14
2.2.5	General parameters .....	14
2.2.6	Numerical parameters .....	14
2.2.7	Comments .....	14
<b>2.3</b>	<b>Results</b>	<b>14</b>
<b>2.4</b>	<b>Conclusion</b>	<b>14</b>
<b>3</b>	<b>Rouse</b>	<b>15</b>
<b>3.1</b>	<b>Purpose</b>	<b>15</b>
<b>3.2</b>	<b>Description</b>	<b>15</b>
3.2.1	Reference .....	15
3.2.2	Geometry and Mesh .....	15
3.2.3	Physical parameters .....	15

3.2.4	Initial and Boundary Conditions .....	16
3.2.5	General parameters .....	16
3.2.6	Numerical parameters .....	16
3.2.7	Comments .....	17
<b>3.3</b>	<b>Results</b>	<b>17</b>
<b>3.4</b>	<b>Conclusion</b>	<b>17</b>
<b>4</b>	<b>V</b> .....	<b>18</b>
<b>4.1</b>	<b>Purpose</b>	<b>18</b>
<b>4.2</b>	<b>Description</b>	<b>18</b>
4.2.1	Reference .....	18
4.2.2	Geometry and Mesh .....	18
4.2.3	Physical parameters .....	19
4.2.4	Initial and Boundary Conditions .....	19
4.2.5	General parameters .....	19
4.2.6	Numerical parameters .....	19
4.2.7	Comments .....	19
<b>4.3</b>	<b>Results</b>	<b>19</b>
<b>4.4</b>	<b>Conclusion</b>	<b>20</b>
<b>5</b>	<b>Viollet</b> .....	<b>21</b>
<b>5.1</b>	<b>Purpose</b>	<b>21</b>
<b>5.2</b>	<b>Description</b>	<b>21</b>
5.2.1	Reference .....	21
5.2.2	Geometry and Mesh .....	21
5.2.3	Physical parameters .....	21
5.2.4	Initial and Boundary Conditions .....	22
5.2.5	General parameters .....	22
5.2.6	Numerical parameters .....	22
5.2.7	Comments .....	22
<b>5.3</b>	<b>Results</b>	<b>22</b>
<b>5.4</b>	<b>Conclusion</b>	<b>23</b>
<b>6</b>	<b>amr</b> .....	<b>24</b>
<b>6.1</b>	<b>Purpose</b>	<b>24</b>
<b>6.2</b>	<b>Description</b>	<b>24</b>
6.2.1	Reference .....	24
6.2.2	Geometry and Mesh .....	24
6.2.3	Physical parameters .....	24
6.2.4	Initial and Boundary Conditions .....	24
6.2.5	General parameters .....	24
6.2.6	Numerical parameters .....	24
6.2.7	Comments .....	24

<b>6.3</b>	<b>Results</b>	<b>24</b>
<b>6.4</b>	<b>Conclusion</b>	<b>24</b>
<b>7</b>	<b>Bergenmeersen test case</b>	<b>25</b>
<b>7.1</b>	<b>Purpose</b>	<b>25</b>
<b>7.2</b>	<b>Description</b>	<b>25</b>
7.2.1	Measurements	27
<b>7.3</b>	<b>Computational options</b>	<b>27</b>
7.3.1	Mesh	27
7.3.2	Initial and boundary conditions	28
7.3.3	Numerical parameters	28
7.3.4	Culvert parameters	28
<b>7.4</b>	<b>Results</b>	<b>29</b>
<b>8</b>	<b>bottom_bc</b>	<b>33</b>
<b>8.1</b>	<b>Purpose</b>	<b>33</b>
<b>8.2</b>	<b>Description of the problem</b>	<b>33</b>
8.2.1	Geometry and Mesh	33
8.2.2	Initial and Boundary Conditions	33
8.2.3	Numerical parameters	33
<b>8.3</b>	<b>Results</b>	<b>34</b>
<b>9</b>	<b>bump</b>	<b>35</b>
<b>9.1</b>	<b>Purpose</b>	<b>35</b>
<b>9.2</b>	<b>Description</b>	<b>35</b>
9.2.1	Reference	35
9.2.2	Geometry and Mesh	35
9.2.3	Physical parameters	36
9.2.4	Initial and Boundary Conditions	36
9.2.5	General parameters	36
9.2.6	Numerical parameters	36
9.2.7	Comments	36
<b>9.3</b>	<b>Results</b>	<b>36</b>
<b>9.4</b>	<b>Conclusion</b>	<b>36</b>
<b>10</b>	<b>bump_static</b>	<b>37</b>
<b>10.1</b>	<b>Purpose</b>	<b>37</b>
<b>10.2</b>	<b>Description</b>	<b>37</b>
10.2.1	Reference	37
10.2.2	Geometry and Mesh	37
10.2.3	Physical parameters	37
10.2.4	Initial and Boundary Conditions	37
10.2.5	General parameters	37

10.2.6	Numerical parameters . . . . .	37
10.2.7	Comments . . . . .	37
<b>10.3</b>	<b>Results</b>	<b>37</b>
<b>10.4</b>	<b>Conclusion</b>	<b>37</b>
<b>11</b>	<b>canal</b> . . . . .	<b>38</b>
<b>11.1</b>	<b>Purpose</b>	<b>38</b>
<b>11.2</b>	<b>Description</b>	<b>38</b>
11.2.1	Reference . . . . .	38
11.2.2	Geometry and Mesh . . . . .	38
11.2.3	Physical parameters . . . . .	39
11.2.4	Initial and Boundary Conditions . . . . .	39
11.2.5	General parameters . . . . .	39
11.2.6	Numerical parameters . . . . .	39
11.2.7	Comments . . . . .	39
<b>11.3</b>	<b>Results</b>	<b>39</b>
<b>11.4</b>	<b>Conclusion</b>	<b>39</b>
<b>12</b>	<b>Schematic culvert test case</b> . . . . .	<b>40</b>
<b>12.1</b>	<b>Purpose</b>	<b>40</b>
<b>12.2</b>	<b>Description</b>	<b>40</b>
<b>12.3</b>	<b>Computational options</b>	<b>40</b>
12.3.1	Mesh . . . . .	40
12.3.2	Initial and boundary conditions . . . . .	40
12.3.3	Numerical parameters . . . . .	41
12.3.4	Culvert characteristics . . . . .	41
<b>12.4</b>	<b>Results</b>	<b>42</b>
<b>13</b>	<b>delwaq</b> . . . . .	<b>44</b>
<b>13.1</b>	<b>Purpose</b>	<b>44</b>
<b>13.2</b>	<b>Description</b>	<b>44</b>
13.2.1	Reference . . . . .	44
13.2.2	Geometry and Mesh . . . . .	44
13.2.3	Physical parameters . . . . .	44
13.2.4	Initial and Boundary Conditions . . . . .	45
13.2.5	General parameters . . . . .	45
13.2.6	Numerical parameters . . . . .	45
13.2.7	Comments . . . . .	45
<b>13.3</b>	<b>Results</b>	<b>45</b>
<b>13.4</b>	<b>Conclusion</b>	<b>45</b>

<b>14</b>	<b>gouttedo</b>	<b>46</b>
<b>14.1</b>	<b>Purpose</b>	<b>46</b>
<b>14.2</b>	<b>Description</b>	<b>46</b>
14.2.1	Reference	46
14.2.2	Geometry and Mesh	46
14.2.3	Physical parameters	46
14.2.4	Initial and Boundary Conditions	47
14.2.5	General parameters	47
14.2.6	Numerical parameters	47
14.2.7	Comments	47
<b>14.3</b>	<b>Results</b>	<b>47</b>
<b>14.4</b>	<b>Conclusion</b>	<b>47</b>
<b>15</b>	<b>Lock-exchange</b>	<b>48</b>
<b>15.1</b>	<b>Purpose</b>	<b>48</b>
<b>15.2</b>	<b>Description</b>	<b>48</b>
<b>15.3</b>	<b>Preamble – an attempt at reproducing Adduce <i>et al.</i>'s experiments</b>	<b>49</b>
<b>15.4</b>	<b>Case setup</b>	<b>49</b>
15.4.1	Geometry and mesh	49
15.4.2	Physical parameters	50
15.4.3	Initial and Boundary Conditions	50
15.4.4	General parameters	50
15.4.5	Numerical parameters	50
<b>15.5</b>	<b>Reference results</b>	<b>51</b>
<b>15.6</b>	<b>Results</b>	<b>52</b>
15.6.1	Dynamic pressure not included in the wave equation	52
15.6.2	Dynamic pressure included in the wave equation	55
15.6.3	Hydrostatic hypothesis	56
<b>15.7</b>	<b>Conclusion</b>	<b>56</b>
<b>16</b>	<b>malpasset</b>	<b>58</b>
<b>16.1</b>	<b>Purpose</b>	<b>58</b>
<b>16.2</b>	<b>Description</b>	<b>58</b>
16.2.1	Reference	58
16.2.2	Geometry and Mesh	58
16.2.3	Physical parameters	59
16.2.4	Initial and Boundary Conditions	59
16.2.5	General parameters	59
16.2.6	Numerical parameters	59
16.2.7	Comments	59
<b>16.3</b>	<b>Results</b>	<b>59</b>
<b>16.4</b>	<b>Conclusion</b>	<b>59</b>

<b>17</b>	<b>particles</b>	<b>60</b>
17.1	Purpose	60
17.2	Description	60
17.2.1	Reference	60
17.2.2	Geometry and Mesh	60
17.2.3	Physical parameters	60
17.2.4	Initial and Boundary Conditions	60
17.2.5	General parameters	60
17.2.6	Numerical parameters	61
17.2.7	Comments	61
17.3	Results	61
17.4	Conclusion	61
<b>18</b>	<b>pildepon</b>	<b>62</b>
18.1	Purpose	62
18.2	Description	62
18.2.1	Reference	62
18.2.2	Geometry and Mesh	62
18.2.3	Physical parameters	62
18.2.4	Initial and Boundary Conditions	62
18.2.5	General parameters	63
18.2.6	Numerical parameters	63
18.2.7	Comments	63
18.3	Results	63
18.4	Conclusion	63
<b>19</b>	<b>plage</b>	<b>64</b>
19.1	Purpose	64
19.2	Description	64
19.2.1	Reference	64
19.2.2	Geometry and Mesh	64
19.2.3	Physical parameters	64
19.2.4	Initial and Boundary Conditions	64
19.2.5	General parameters	65
19.2.6	Numerical parameters	65
19.2.7	Comments	65
19.3	Results	65
19.4	Conclusion	65
<b>20</b>	<b>pluie</b>	<b>66</b>
20.1	Purpose	66
20.2	Description	66
20.2.1	Reference	66
20.2.2	Geometry and Mesh	66

20.2.3	Physical parameters . . . . .	66
20.2.4	Initial and Boundary Conditions . . . . .	66
20.2.5	General parameters . . . . .	67
20.2.6	Numerical parameters . . . . .	67
20.2.7	Comments . . . . .	67
<b>20.3</b>	<b>Results</b>	<b>67</b>
<b>20.4</b>	<b>Conclusion</b>	<b>67</b>
<b>21</b>	<b>Solitary wave . . . . .</b>	<b>68</b>
<b>21.1</b>	<b>Purpose</b>	<b>68</b>
<b>21.2</b>	<b>Notations</b>	<b>68</b>
<b>21.3</b>	<b>Theory</b>	<b>68</b>
<b>21.4</b>	<b>Description</b>	<b>69</b>
21.4.1	Geometry and Mesh . . . . .	69
21.4.2	Physical parameters . . . . .	70
21.4.3	Initial and Boundary Conditions . . . . .	70
21.4.4	General parameters . . . . .	70
21.4.5	Numerical parameters . . . . .	70
<b>21.5</b>	<b>Results</b>	<b>71</b>
<b>21.6</b>	<b>Conclusion</b>	<b>72</b>
<b>22</b>	<b>source . . . . .</b>	<b>73</b>
<b>22.1</b>	<b>Purpose</b>	<b>73</b>
<b>22.2</b>	<b>Description</b>	<b>73</b>
22.2.1	Reference . . . . .	73
22.2.2	Geometry and Mesh . . . . .	73
22.2.3	Physical parameters . . . . .	73
22.2.4	Initial and Boundary Conditions . . . . .	73
22.2.5	General parameters . . . . .	74
22.2.6	Numerical parameters . . . . .	74
22.2.7	Definition of sources . . . . .	74
22.2.8	Comments . . . . .	74
<b>22.3</b>	<b>Results</b>	<b>74</b>
<b>22.4</b>	<b>Conclusion</b>	<b>79</b>
<b>23</b>	<b>stratification . . . . .</b>	<b>80</b>
<b>23.1</b>	<b>Purpose</b>	<b>80</b>
<b>23.2</b>	<b>Description</b>	<b>80</b>
23.2.1	Reference . . . . .	80
23.2.2	Geometry and Mesh . . . . .	80
23.2.3	Physical parameters . . . . .	80
23.2.4	Initial and Boundary Conditions . . . . .	81
23.2.5	General parameters . . . . .	81
23.2.6	Numerical parameters . . . . .	81

23.2.7	Comments .....	81
<b>23.3</b>	<b>Results</b>	<b>81</b>
<b>23.4</b>	<b>Conclusion</b>	<b>81</b>
<b>24</b>	<b>tetra</b> .....	<b>82</b>
<b>24.1</b>	<b>Purpose</b>	<b>82</b>
<b>24.2</b>	<b>Description</b>	<b>82</b>
24.2.1	Reference .....	82
24.2.2	Geometry and Mesh .....	82
24.2.3	Physical parameters .....	82
24.2.4	Initial and Boundary Conditions .....	83
24.2.5	General parameters .....	83
24.2.6	Numerical parameters .....	83
24.2.7	Comments .....	83
<b>24.3</b>	<b>Results</b>	<b>83</b>
<b>24.4</b>	<b>Conclusion</b>	<b>83</b>
<b>25</b>	<b>thomson</b> .....	<b>84</b>
<b>25.1</b>	<b>Purpose</b>	<b>84</b>
<b>25.2</b>	<b>Description</b>	<b>84</b>
25.2.1	Reference .....	84
25.2.2	Geometry and Mesh .....	84
25.2.3	Physical parameters .....	84
25.2.4	Initial and Boundary Conditions .....	85
25.2.5	General parameters .....	85
25.2.6	Numerical parameters .....	85
25.2.7	Comments .....	85
<b>25.3</b>	<b>Results</b>	<b>85</b>
<b>25.4</b>	<b>Conclusion</b>	<b>85</b>
<b>26</b>	<b>tide</b> .....	<b>86</b>
<b>26.1</b>	<b>Purpose</b>	<b>86</b>
<b>26.2</b>	<b>Description</b>	<b>86</b>
26.2.1	Reference .....	86
26.2.2	Geometry and Mesh .....	86
26.2.3	Physical parameters .....	86
26.2.4	Initial and Boundary Conditions .....	87
26.2.5	General parameters .....	87
26.2.6	Numerical parameters .....	87
26.2.7	Comments .....	87
<b>26.3</b>	<b>Results</b>	<b>87</b>
<b>26.4</b>	<b>Conclusion</b>	<b>87</b>

<b>27</b>	<b>uneven</b>	<b>88</b>
27.1	Purpose	88
27.2	Description	88
27.2.1	Reference	88
27.2.2	Geometry and Mesh	88
27.2.3	Physical parameters	88
27.2.4	Initial and Boundary Conditions	88
27.2.5	General parameters	89
27.2.6	Numerical parameters	89
27.2.7	Comments	89
27.3	Results	89
27.4	Conclusion	89
<b>28</b>	<b>vasque</b>	<b>90</b>
28.1	Purpose	90
28.2	Description	90
28.2.1	Reference	90
28.2.2	Geometry and Mesh	90
28.2.3	Physical parameters	90
28.2.4	Initial and Boundary Conditions	90
28.2.5	General parameters	91
28.2.6	Numerical parameters	91
28.2.7	Comments	91
28.3	Results	91
28.4	Conclusion	91
<b>29</b>	<b>vent</b>	<b>92</b>
29.1	Purpose	92
29.2	Description	92
29.2.1	Reference	92
29.2.2	Geometry and Mesh	93
29.2.3	Physical parameters	93
29.2.4	Initial and Boundary Conditions	93
29.2.5	General parameters	93
29.2.6	Numerical parameters	93
29.2.7	Comments	93
29.3	Results	93
29.4	Conclusion	94
	Bibliography	95

# 1. Cooper

## 1.1 Purpose

This test demonstrates the ability of TELEMAC-3D to model the buoyancy of an active tracer.

## 1.2 Description

We consider a square channel of 4,000 m side with a flat bottom at  $z = -10$  m with a bump at  $z = -6$  m in the middle ( $x = 2,000$  m;  $y = 2,000$  m) (cf. figure 3.15.1). The source of tracer is located above the bump at  $z = -5$  m.

We observe the buoyancy of the active tracer.

### 1.2.1 Reference

### 1.2.2 Geometry and Mesh

#### Bathymetry

Flat bottom at  $z = -10$  m with a bump at  $z = -6$  m in the middle of the domain.

#### Geometry

Channel length = 4,000 m

Channel width = 4,000 m

#### Mesh

3,204 triangular elements

1,683 nodes

11 fixed planes regularly spaced

### 1.2.3 Physical parameters

Constant diffusion of velocity:

- Horizontal:  $10^{-4}$  m<sup>2</sup>/s,
- Vertical: no.

Constant diffusion of tracer:

- Horizontal: no,
- Vertical: 0.1 m<sup>2</sup>/s.

Tracer density law specifying a  $\beta$  spatial expansion coefficient of  $0.0003\text{ K}^{-1}$  and a standard value of the tracer of 0.0.

Coriolis: no

Wind: no

#### 1.2.4 Initial and Boundary Conditions

##### Initial conditions

Constant water level at  $z = 0\text{ m}$

Initial value of tracer = 0

##### Boundary conditions

Closed boundaries

Bottom friction: Nikuradse's formula with asperities of  $0.01\text{ m}$

Tracer discharge at source:  $20.0\text{ m}^3/\text{s}$

Tracer value at source:  $333.33\text{ g/L}$  or  $\text{kg/m}^3$

#### 1.2.5 General parameters

Time step: 5 s

Simulation duration: 1,800 s (30 min)

#### 1.2.6 Numerical parameters

Non-hydrostatic version

Advection of velocities and tracer: N-type MURD scheme

#### 1.2.7 Comments

The tested parameters file is "t3d\_cooper.cas". The steering files "t3d\_cooper-hyd.cas" & "t3d\_cooper-supg.cas" are only used as non-regression validation.

### 1.3 Results

Figure 3.15.2 highlights that the buoyancy of the active tracer generates vertical velocities, thus establishing a large recirculation around the bump. This is not due to the injected flow rate. Mass balance of the log file after 1,800 s:

```
--- WATER ---
INITIAL MASS : 0.1598743E+09
FINAL MASS : 0.1599103E+09
MASS LEAVING THE DOMAIN (OR SOURCE) : -36000.00
MASS LOSS : 0.4833937E-04
--- TRACER 1 ---
INITIAL MASS : 0.000000
FINAL MASS : 0.1199988E+08
MASS EXITING (BOUNDARIES OR SOURCE) : -0.1199988E+08
MASS LOSS : -0.5826335E-03
```

The amount of water injected by the source is correct:  $20\text{ m}^3/\text{s} \times 1,800\text{ s} = 36,000\text{ m}^3$  The amount of tracer injected is correct:  $333.33\text{ kg/m}^3 \times 20\text{ m}^3/\text{s} \times 1,800\text{ s} = 1.19999 \times 10^7\text{ kg}$

### 1.4 Conclusion

TELEMAC-3D simulates correctly the buoyancy of an active tracer.

## 2. NonLinearWave

### 2.1 Purpose

This test demonstrates the ability of TELEMAC-3D to simulate the evolution of a monochromatic linear wave over a bar. This test case corresponds to a physical model and measurements published by Dingemans (conditions C) [1].

### 2.2 Description

We consider a tank 32 m long and 0.3 m wide. The evolution of the topography along the channel is presented on figure 3.13.1. A wave is imposed at the entrance of the channel. The goal is to simulate the evolution of this wave when propagating over the bar.

The simulation is made with and without hydrostatic hypothesis.

#### 2.2.1 Reference

[1] DINGEMANS M.W., Comparison of computations with Boussinesq-like models and laboratory measurements. MAST-G8M note, H1684, Delft Hydraulics, 32 pp. 1994.

[2] BENOIT M., Projet CLAROM-ECOMAC (FICHE CEP&M M06101.99). Modélisation non-linéaire par les équations de Boussinesq de la propagation des vagues non-déferlantes en zone côtière. Rapport EDF-LNHE HP-75/01/069. 2001.

#### 2.2.2 Geometry and Mesh

##### Bathymetry

Representing a bar (see figure 3.13.1)

##### Geometry

Channel length = 32 m

Channel width = 0.3 m

##### Mesh

7,680 triangular elements

5,124 nodes

10 planes regularly spaced

### 2.2.3 Physical parameters

Diffusion: no

Coriolis: no

Wind: no

### 2.2.4 Initial and Boundary Conditions

#### Initial conditions

Initial free surface at level 0.

No velocity

#### Boundary conditions

Closed lateral boundaries. No bottom friction

Imposed wave at the entrance (amplitude 0.04 m)

### 2.2.5 General parameters

Time step: 0.0025 s

Simulation duration: 33 s

### 2.2.6 Numerical parameters

Non-hydrostatic version

Advection of velocities: N-type MURD scheme

### 2.2.7 Comments

#### 2.3 Results

Figure 3.13.1 presents the general shape of the free surface at the end of the simulation.

Figure 3.13.2 presents a comparison of the TELEMAC simulation and the experimental results at various locations in the channel. This comparison shows a very good agreement between results and measurements which is comparable to the one obtained with 1D Boussinesq models as published in reference [2].

### 2.4 Conclusion

TELEMAC-3D simulates correctly the evolution of a wave on a bar.

## 3. Rouse

### 3.1 Purpose

This test validates the modeling of the hydrodynamics and non-cohesive suspended sediment transport, in a permanent and uniform flow. We compare the mean flow velocities to the logarithmic profile and the sediment concentration to an analytical solution derived from the Rouse profile [1].

### 3.2 Description

It consists of a steady and uniform flow in a rectangular channel ( $500\text{ m} \times 100\text{ m}$ ) with constant slope, without friction on the lateral boundaries, and with friction on the bottom. The turbulence model is chosen to be consistent with the logarithmic velocity profile on the vertical. At the entrance of the channel, sediment is introduced with a constant concentration along the vertical, and an equilibrium profile gradually appears downstream.

#### 3.2.1 Reference

[1] HERVOUET J.-M., VILLARET C. Profil de Rouse modifié, une solution analytique pour valider TELEMAC-3D en sédimentologie. EDF-LNHE Report HP-75/04/013/A.

#### 3.2.2 Geometry and Mesh

##### Bathymetry

Constant slope of  $1.01 \cdot 10^{-3}$  (at  $x = 0\text{ m}$ ,  $z = 0\text{ m}$  and at  $x = 500\text{ m}$ ,  $z = -0.505\text{ m}$ ) (designed so as to get a uniform flow with a Strickler coefficient equal to  $50\text{ m}^{1/3}/\text{s}$  when the depth is  $0.5\text{ m}$ )

##### Geometry

Channel length =  $500\text{ m}$

Channel width =  $100\text{ m}$

##### Mesh

2,204 triangular elements

1,188 nodes

16 planes irregularly spaced (zstar) on the vertical (see figure 3.17.1)

#### 3.2.3 Physical parameters

Turbulence:

- Horizontal : Constant viscosity of  $0.1 \text{ m}^2/\text{s}$
- Vertical : Nezu and Nakagawa mixing length model

Coriolis: no

Wind: no

Sediment of mean diameter of 6 mm with a settling velocity of -0.01 m/s

No influence of turbulence on sediment settling velocity

Laminar diffusivity of sediment of  $10^{-4} \text{ m}^2/\text{s}$  for the vertical direction ( $10^{-6} \text{ m}^2/\text{s}$  for the horizontal directions)

### 3.2.4 Initial and Boundary Conditions

#### Initial conditions

Constant water depth of 0.5 m

Initial sediment concentration: 0.02 g/L

Velocity and total viscosity field initialised with a logarithmic profile along the vertical (see figure 3.17.2 and 3.17.3)

#### Boundary conditions

Upstream:

- prescribed flow rate of  $50 \text{ m}^3/\text{s}$
- logarithmic velocity profile
- prescribed constant sediment concentration of 0.02 g/L

Downstream:

- prescribed free surface at  $z = -0.005 \text{ m}$
- logarithmic velocity profile

Bottom: solid boundary with Nikuradse bed roughness of  $k_s = 0.0162 \text{ m}$  (equivalent to a Strickler coefficient of  $50 \text{ m}^{1/3}/\text{s}$  at the depth of 0.5 m)

Lateral wall: no friction

### 3.2.5 General parameters

Time step: 2 s

Simulation duration: 2,000 s

### 3.2.6 Numerical parameters

Hydrostatic computation

Advection for velocities and sediment: Characteristics

### 3.2.7 Comments

#### 3.3 Results

Figure 3.17.5 compares the theoretical [1] (i.e. logarithmic) velocity profile with the computed result and shows an excellent agreement. One can see that the point at the first plane above the bottom coincides with the theoretical value, which guarantees that the friction velocity is correct.

Figure 3.17.6 compares the theoretical [1] and the computed turbulent viscosity profiles. The maximum error happens at the first two planes below the surface (perhaps because of the size of the mesh at this level).

Figure 3.17.7 compares the classic theoretical Rouse profile, the modified Rouse profile [1], and the numerical solution obtained with a laminar viscosity of  $10^{-4} \text{ m}^2/\text{s}$ . The numerical solution is close to the modified profile. In theory, the Rouse profile is only valid beyond the viscous layer. The modified profile brings a notable modification only in this viscous layer and is presented here for its interest in software validation.

### 3.4 Conclusion

These comparisons with analytical solutions, in hydrodynamics or suspended sediment transport, thoroughly validate the treatment of diffusion on the vertical in TELEMAC-3D, including a settling velocity. The Nezu and Nakagawa mixing length turbulence model, and the computation of velocity gradients, is also validated.

## 4. V

### 4.1 Purpose

The purpose of this test is to verify the validity of the diffusion step and the proper treatment of the buoyancy terms. Moreover, this test demonstrates the ability of TELEMAC-3D to model a vertical stratification induced by an active tracer distribution on a non-horizontal topography. A closed rectangular channel is initialised with such vertical tracer distribution without motion. This stratification is stable and the distribution of the tracer should not evolve in time neither generate any flow. The test case is treated with both prism and tetrahedron elements.

### 4.2 Description

The considered domain is a horizontal V-shaped channel. The horizontal mesh is composed of triangular cells nearly homogenous in size. The test case is first solved using a vertical mesh of prismatic cells fitting the topography, and in a second time using tetrahedron elements. The horizontal and vertical meshes are presented on figure 3.2.1. The active tracer is the temperature with a corresponding value of the thermal expansion coefficient  $\beta = 2.10^{-4} \text{ K}^{-1}$  (see the User's Manual).

#### 4.2.1 Reference

#### 4.2.2 Geometry and Mesh

##### Bathymetry

Bottom at -13 m in the centre of the channel

Bottom at 0 m on the side of the channel banks

Linearly interpolated depth between the centre and the banks

The bathymetry can be observed on figure 3.2.1 (with an expansion factor on the vertical equal to 10)

##### Geometry

Channel length = 500 m

Channel width = 100 m

##### Mesh

648 triangular elements

373 nodes

11 planes regularly spaced in the vertical direction  
 Prism or tetrahedron elements

#### 4.2.3 Physical parameters

Constant horizontal viscosity  $1 \text{ m}^2/\text{s}$ , and tracer diffusion  $1 \text{ m}^2/\text{s}$   
 Temperature density law specifying an expansion coefficient  $\beta = 2.10^{-4} \text{ K}^{-1}$   
 No vertical viscosity  
 Coriolis: no  
 Wind: no

#### 4.2.4 Initial and Boundary Conditions

##### Initial conditions

No velocity  
 Constant initial water level at  $z = 0.1 \text{ m}$   
 Tracer initialised as  $T = 10 + z/1.3 \text{ }^\circ\text{C}$

##### Boundary conditions

Channel banks: slip solid boundary  
 Bottom: slip solid boundary  
 Tracer: no flux through the bottom and the free surface

#### 4.2.5 General parameters

Time step: 0.1 s  
 Simulation duration: 1 s

#### 4.2.6 Numerical parameters

Non-hydrostatic computation  
 Advection for velocities: Explicit Leo Postma scheme  
 Advection for tracer: Explicit Leo Postma scheme

#### 4.2.7 Comments

### 4.3 Results

During the simulation, the vertical profile of tracer concentration is stable for both computations (see figure 3.2.2 and 3.2.4). However, at the end of the computation with prism elements, some negligible differences on the temperature field (maximum value for example, up to 0.01 %) are observed. Figure 3.2.3 shows disturbance of velocity field negligible (of the order of  $10^{-7}$ ) for the prism elements computation. This velocity field is connected to the difficulty to build the diffusion matrix using prismatic elements. The computation with tetrahedron elements (see figure 3.2.5) shows some very negligible (of the order of  $10^{-16}$ ) disturbance of the velocity field. In any case, the situation can be considered as globally stable. The test is done essentially to verify the horizontal diffusion terms, which are estimated in the transformed  $\sigma$ -mesh (buoyancy terms). In this case, the tracer does not induce any flow. The final mass balance of computation using prism elements exposes a very good mass conservation (the total mass loss is less than  $0.5 \cdot 10^{-6}$ ). For the computation using tetrahedron elements, the conservation of mass and temperature is perfect.

#### 4.4 Conclusion

The diffusion equation of tracers is properly solved by TELEMAC-3D. The buoyancy terms are properly taken into account for a linear vertical tracer distribution. Unlike tetrahedron elements computation, using prism elements generates a small disturbance of the velocity field and some negligible differences on the temperature field. Nevertheless, the generated disturbance is small with respect to the vertical gradient of the tracer and is principally due to machine precision and diffusion matrix treatment. The tracer is still stable at the end of the simulation.

## 5. Viollet

### 5.1 Purpose

This test demonstrates the ability of TELEMAC-3D to model thermal and stratified flow.

### 5.2 Description

The test case considers the stable configuration of Pierre-Louis Viollet's experimentation (1980) with a Froude number of 0.9, which consists in a 2 layer flow of same height,  $h = 0.1$  m. The lower layer has a velocity  $U_2$  and a temperature  $T_2$ . The upper layer has a velocity  $U_1 < U_2$  and a temperature  $T_1 > T_2$ .

#### 5.2.1 Reference

#### 5.2.2 Geometry and Mesh

##### Bathymetry

Channel tilt =  $5.30921 \times 10^{-6}$  (see figure 3.18.2)

##### Geometry

Channel length = 10 m ( $100h$ )

Channel width = 1 m ( $10h$ )

##### Mesh

1280 triangular elements (see figure 3.18.2)

697 nodes

27 planes regularly spaced on the vertical ( $\sigma$  transformation).

#### 5.2.3 Physical parameters

Turbulence:  $k-\varepsilon$  in both directions

Prandtl number: 0.71

Karman constant: 0.41

Bottom friction: Haaland law with coefficient equal to 63.4505112

Density law is a function of temperature.

### 5.2.4 Initial and Boundary Conditions

#### Initial conditions

$U_1 = 0.05 \text{ m/s}$   $T_1 = 25.35^\circ\text{C}$

$U_2 = 0.05 \text{ m/s}$   $T_2 = 20^\circ\text{C}$

Constant height of 0.2 m ( $2h$ )

#### Boundary conditions

Closed boundaries on sides.

Upstream prescribed flow rate:  $0.01 \text{ m}^3/\text{s}$

Downstream prescribed water level:  $0.19995 \text{ m}$

A double logarithmic velocity profile is imposed for the lower layer and a logarithmic profile for the upper layer (see figure 3.18.1) according the following formulae defined in the BORD3D subroutine:

where  $z_1$  and  $z_2$  are the levels in upper and lower layers respectively (starting from the lower level of each layer).  $\xi_s = 10^{-4} \text{ m}$  et  $dz$  is the distance between two planes (i.e.  $dz = h/26$  since there are 27 planes).

Upstream  $k$  and  $\varepsilon$  profiles are imposed according the following formulae defined in the KEPCL3 subroutine:

where  $n_{turb} = 5 \times 10^{-3}$ ,  $C_\mu = 0.09$  and  $\delta = 10^{-6}$

Surface and bottom boundary condition for  $\varepsilon$  are defined in the KEPICL subroutine: Neumann at bottom and Dirichlet at surface.

### 5.2.5 General parameters

Time step: 0.1 s

Simulation duration: 500 s (8 min 20 s)

### 5.2.6 Numerical parameters

Non-hydrostatic computation

Advection of velocities, temperature and  $k$ - $\varepsilon$ : N-type MURD scheme

### 5.2.7 Comments

It should be noted that a bias exists in the measures presented: the channel inlet flow does not correspond to the integral of the measured speeds on the section. This comes probably from measurement error of the velocity field. The velocity been the field that is sought to be reproduced, the measured velocity field is corrected by multiplying it by a constant. No correction is applied to temperature measurements.

## 5.3 Results

Figure 3.18.3 presents velocity and temperature profiles comparisons at  $x/h = 10, 30$  and  $100$  between TELEMAC-3D results and corrected experimental measurement of P-L Viollet, for the stable stratification case with  $Fr = 0.9$ .

The comparisons show a good match between simulation results and measurements. The evolution of the velocity and temperature profiles at the different sections of the channel is well reproduced.

**5.4 Conclusion**

TELEMAC-3D is capable to model thermal and stratified flow.

## **6. amr**

**6.1 Purpose**

**6.2 Description**

**6.2.1 Reference**

**6.2.2 Geometry and Mesh**

Bathymetry

Geometry

Mesh

**6.2.3 Physical parameters**

**6.2.4 Initial and Boundary Conditions**

Initial conditions

Boundary conditions

**6.2.5 General parameters**

**6.2.6 Numerical parameters**

**6.2.7 Comments**

**6.3 Results**

**6.4 Conclusion**

## 7. Bergenmeersen test case

### 7.1 Purpose

The purpose of this test-case is to test the culvert functionality in TELEMAC-3D with a quantitative comparison to measurements of the flow rates through the culverts and the water levels on each side of the culverts.

### 7.2 Description

A recent (2013) example of the implementation of a Flood Control Area (FCA) with a controlled reduced tide (CRT) system is located in Bergenmeersen. The ring dike that surrounds the FCA has a crest level of 8 m TAW (Tweede Algemene Waterpassing, the reference level in Belgium; 0 m TAW corresponds to the average sea level at low water in Ostende port) and the overflow dike has a crest level of 6.8 m TAW. The configuration used for the inlet and outlet culverts is shown in the Figure 7.1. Three outlet culverts were built to add to other older three outlet culverts that existed in the area. Above the new outlet culverts, six new inlet culverts were built and at their entrance weirs (i.e. wooden beams) with different heights were added (Figure 7.1 and Figure 7.2). At each inlet and outlet culvert the flow is separated into two parts at the entrance of the culvert by a kind of pilar and then converges again right after this pilar. Figure 7.3 shows an example of the trash screens that are present. Table 7.1 gives an overview of the characteristics of these new inlet and outlet culverts.

To test the new culvert functionality implemented in TELEMAC-3D this new configuration of in- and outlet culverts is tested. The quality of the results can be assessed compared to measurements of the mean water levels inside the flood control area, outlet discharges, inlet discharges and mean water levels in the river side.

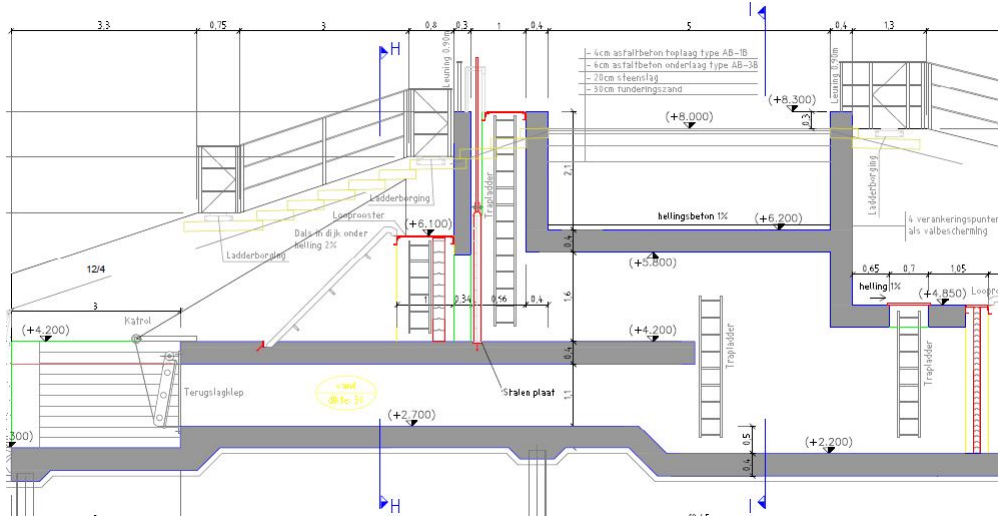


Figure 7.1: Bergenmeersen test case: detail of the side view of the construction of the new inlet and outlet culverts in Bergenmeersen.



Figure 7.2: Bergenmeersen test case: inlet and outlet culvert configuration on the river side (construction phase) (Patrimoniumdatabank W&Z).



Figure 7.3: Bergenmeersen test case: View on the inlet culverts from the river side and inlet and outlet culverts from the FCA side.

Table 7.1: Characteristics of the new inlet and outlet culverts of the new FCA/CRT in Bergenmeersen.

	Inlet (Scheldt side)	Inlet (FCA side)	Outlet (Scheldt side)	Outlet (FCA side)
<b>Number of culverts</b>	6		3	
<b>Culvert width (m)</b>	2.7		3	
<b>Culvert length (m)</b>	9.5		18	
<b>Culvert height (m)</b>	1.6	2.25	1.1	2.25
<b>Level of culvert floor (m TAW)</b>	4.2	2.2	2.7	2.2
<b>Crest level of weirs (m TAW)</b>	4.2/4.2/4.2/ 4.35/4.5/4.5			

### 7.2.1 Measurements

The quality of the numerical results can be assessed compared to measurements of the mean water levels inside the flood control area, outlet discharges, inlet discharges and mean water levels in the river side. Measurements were performed by Flanders Hydraulic Research in Bergenmeersen within a 13 hour campaign during the 10th September, 2013. They obtained water levels in front of the culverts in the Scheldt and in the floodplain sides and discharges for the inlet and outlet culverts. The model results for this period will be compared with the measurements.

## 7.3 Computational options

### 7.3.1 Mesh

The mesh of the computational domain is shown in Figure 7.4. The mesh is cut out of an early version of the Scaldis model. It has a resolution of about 8 m in the river side, and 10 m in the floodplain. Five horizontal layers are uniformly imposed in the model. Detailed bathymetric/topographic data from 2013 is available and used for this model.

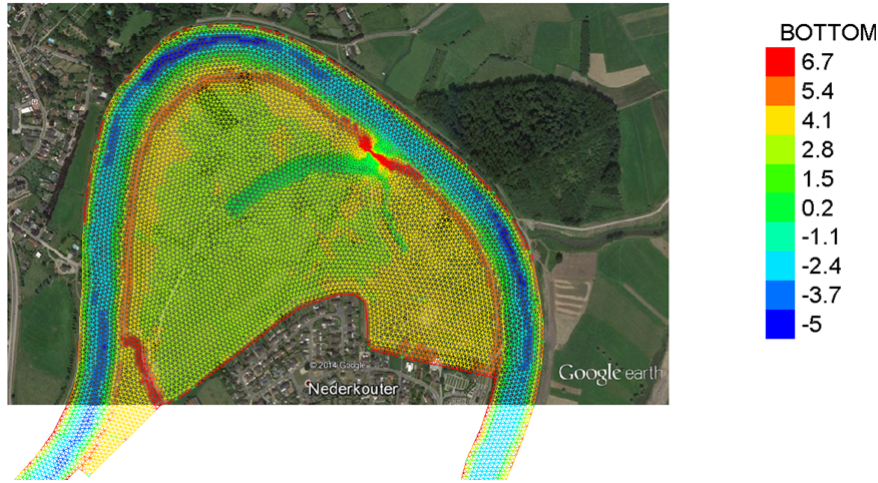


Figure 7.4: Planview of the computational domain to model the FCA/CRT in Bergenmeersen. The colour scale represents de bottom values (m TAW).

### 7.3.2 Initial and boundary conditions

The water levels in the Scheldt river are obtained at the Wetteren tidal station. These values are used as the downstream boundary condition for the hydrodynamic model. Upstream a discharge boundary condition is imposed.

### 7.3.3 Numerical parameters

The simulation time is about one day (10th September 2014) corresponding to the time period for which measurements of mean water levels were available. The time step is set to 5 seconds, providing, together with the chosen mesh resolution, a stable simulation.

The bottom friction is taken into account in the model through the Manning Strickler's parameter  $n$ , set to  $0.02\text{s} \cdot \text{m}^{-1/3}$ . The horizontal and vertical turbulence viscosity coefficients are both set to  $0.01\text{m}^2\text{s}^{-1}$ .

### 7.3.4 Culvert parameters

Table 7.2 shows the file that the user has to give to TELEMAC-3D in order to take into account the culverts for this FCA with CRT in the Bergenmeersen test case. Besides this new structure there were already in the area three outlet sluices also represented in the input text file as outlet 3 to outlet 6 (information for these outlet sluices is obtained from the Patrimoniumdatabank W&Z) Once again the different head loss coefficients are used to calibrate the model with the experimental data. Most of the parameters are maintained comparatively with the Lippensbroek test case. But there are some exceptions, given the fact that the inlet and outlet culvert configurations are also different. For instance the head loss coefficients at the entrance of the inlet are increased in order to take into account the effect of the flow being split into two parts by a pillar. Following the expression given by Carlier (1972), the head loss due to the presence of pillars is about  $C_p \approx 0.4$  and therefore  $CE_1$  becomes  $CE_1 = C_1 + C_p$ . There is also at the exit of the outlet sluices the separation of the flow into two parts. This effect is taken into account in the head loss due to a valve, increasing the value for  $CV$ . Also during the measurement campaign, the trash screens at the inlet sluices are not cleaned and therefore this coefficient is increased both for the inlet and outlet sluices.

Table 7.2: Input data for the culvert subroutine in TELEMAC-3D to model the Bergenmeersen FCA/CRT.

	<b>CE1</b>	<b>CE2</b>	<b>CS1</b>	<b>CS2</b>	<b>CV</b>	<b>CT</b>	<b>C56</b>	<b>C5</b>	<b>CV5</b>	<b>W</b>	<b>D1</b>	<b>D2</b>	<b>N</b>	<b>L</b>	<b>CP</b>
<b>Inlet 1</b>	0.9	0.5	1	1	0	1	10	6	0	2.7	1.45	2.25	0.015	9.5	0
<b>Inlet 2</b>	0.9	0.5	1	1	0	1	10	6	0	2.7	1.6	2.25	0.015	9.5	0
<b>Inlet 3</b>	0.9	0.5	1	1	0	1	10	6	0	2.7	1.6	2.25	0.015	9.5	0
<b>Inlet 4</b>	0.9	0.5	1	1	0	1	10	6	0	2.7	1.6	2.25	0.015	9.5	0
<b>Inlet 5</b>	0.9	0.5	1	1	0	1	10	6	0	2.7	1.6	2.25	0.015	9.5	0
<b>Inlet 6</b>	0.9	0.5	1	1	0	1	10	6	0	2.7	1.6	2.25	0.015	9.5	0
<b>Outlet 1</b>	0.5	0.5	1	1	12	1	10	6	1.5	3	1.1	2.25	0.015	18.5	2
<b>Outlet 2</b>	0.5	0.5	1	1	12	1	10	6	1.5	3	1.1	2.25	0.015	18.5	2
<b>Outlet 3</b>	0.5	0.5	1	1	12	1	10	6	1.5	3	1.1	2.25	0.015	18.5	2
<b>Outlet 4</b>	0.5	0.5	1	1	12	1	10	6	1.5	1.5	1.8	2.55	0.015	20	2
<b>Outlet 5</b>	0.5	0.5	1	1	12	1	10	6	1.5	1.5	1.8	2.6	0.015	20	2
<b>Outlet 6</b>	0.5	0.5	1	1	12	1	10	6	1.5	1.5	1.8	2.55	0.015	20	2

## 7.4 Results

Figure 7.5 shows the differences in water level in the river in front of the in- and outlet construction of Bergenmeersen. This figure shows that it is difficult to get the water levels in this model correct. The downstream water level boundary of this small model is not located at the same location as the Wetteren tidal measurement station, but more upstream. Keeping this in mind Figure 7.6 shows the difference between measured and modeled water levels in the floodplain. The water level in the model follows a similar path as the measured water level. Given the complicated construction (in terms of translating this to an equation for discharge) of the in- and outlet structure, these results are a good approximation of reality. In Figure 7.7 we see that the outlet discharge computed by the model fits fairly well the experimental data even if the numerical results overestimate the measurements around 12h. Regarding the inlet discharge, Figure 7.8 shows that the computed discharges are overestimated by the model, resulting on the overestimation seen in the mean water level in the FCA. A possible explanation for the discrepancies is that the inlet sluices have gates incorporated and in this test case it is considered that these gates are completely open. We have heard that in reality this is not the case and that the opening of these gates is changed several times over the last two years. The purpose of these gates is to close the area and prevent water from entering. There is no information on the openings of these gates at the time of this 13 hour measurement campaign.

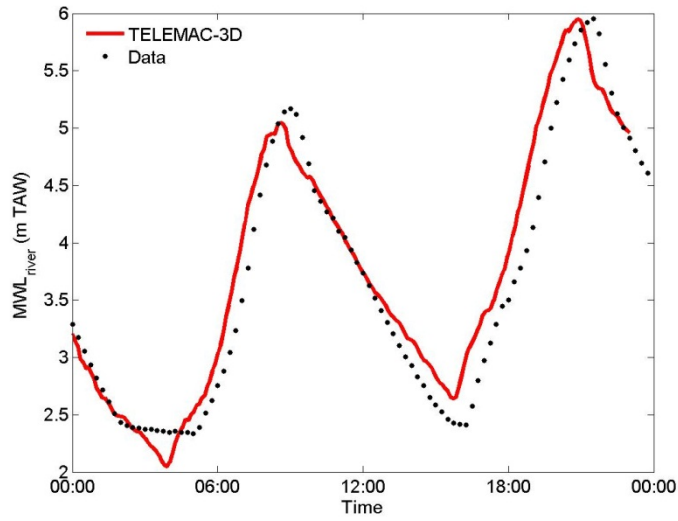


Figure 7.5: Bergenmeersen test case: comparison of the mean water level time evolution in the river between numerical results and measurements.

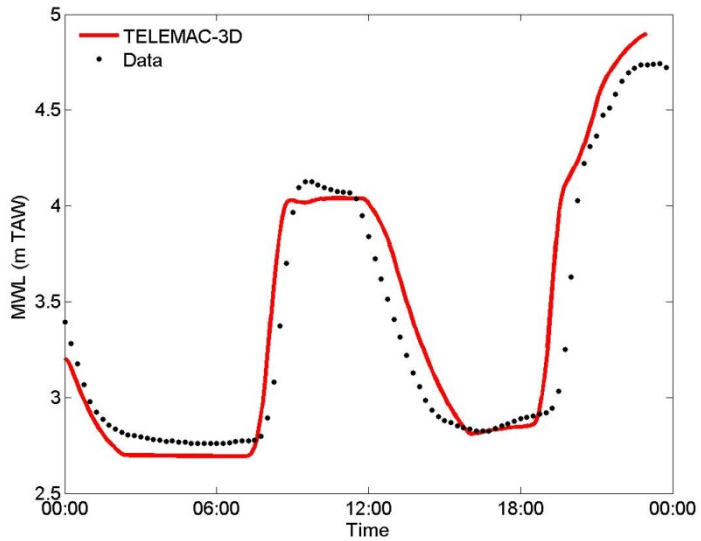


Figure 7.6: Bergenmeersen test case: comparison of the mean water level time evolution in the floodplain between numerical results and measurements.

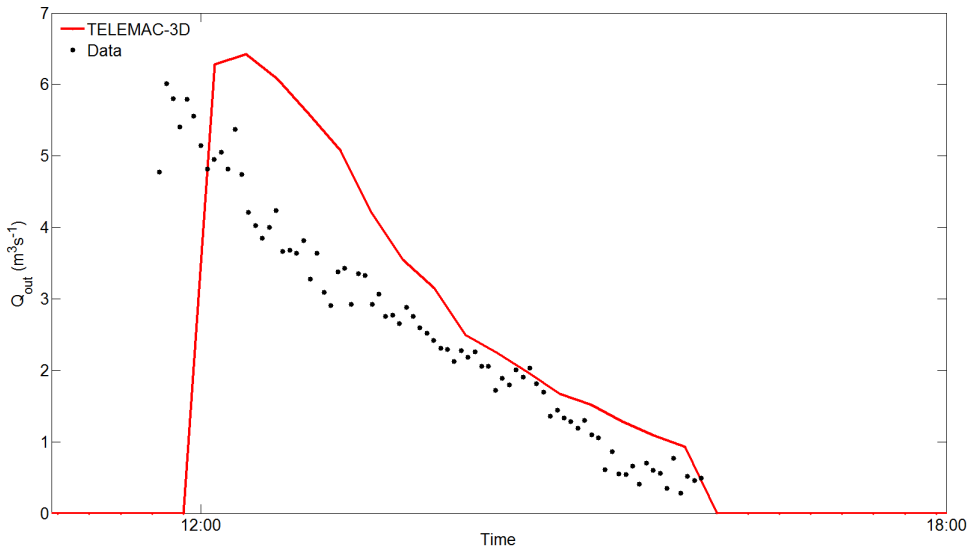


Figure 7.7: Bergenmeersen test case: comparison of outlet culvert discharges time evolution between numerical results and measurements.

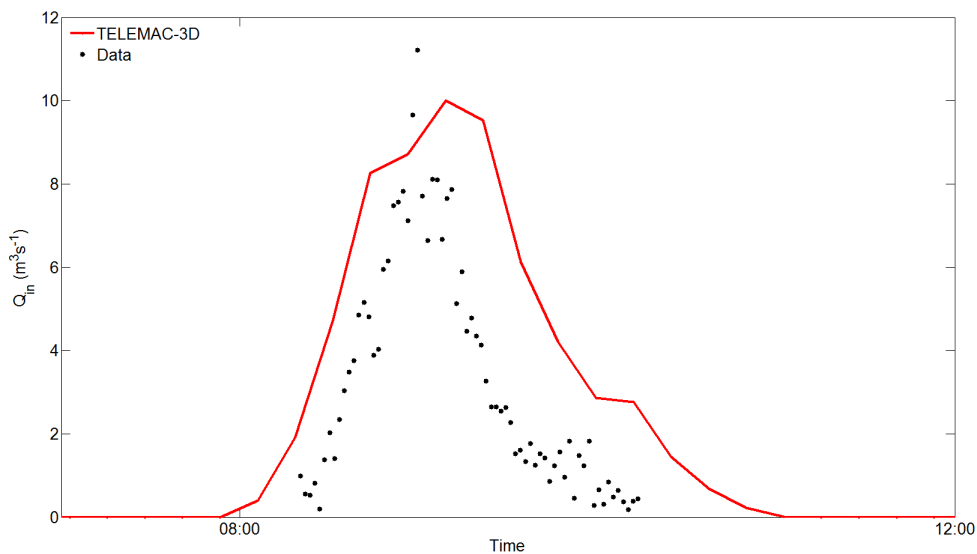


Figure 7.8: Bergenmeersen test case: comparison of inlet culvert discharges time evolution between numerical results and measurements.

The normalized root mean square error is calculated for the mean water levels, outlet and inlet discharges (Table 7.3).

Table 7.3: Normalized root mean square error for the mean water level (MWL\_error), outlet discharge(Qout\_error) and inlet discharge (Qin\_error) in the Bergenmeersen test case.

<b>MWL_error</b>	0.275
<b>Qout_error</b>	0.453
<b>Qin_error</b>	0.538

In Figure 7.9, the flow types that predominate through the inlet and outlet culverts are presented. While for the former, flow types 2, 3 and 4 predominate, for the latter flow types 2 and 4 are the ones that occur the most.

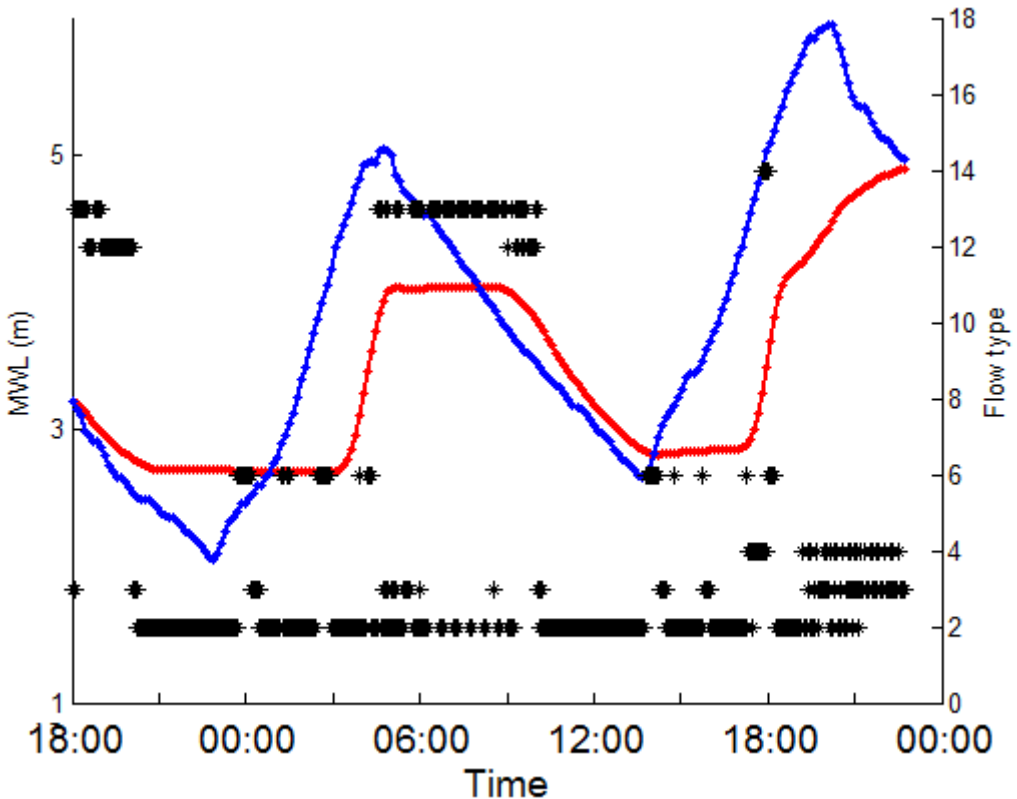


Figure 7.9: Bergenmeersen test case: mean water levels modelled by TELEMAC-3D in the river (blue line) and in the FCA (red line) and the corresponding flow types that occur during the time series. Flow through inlet culvert (type 2 - 6) and through outlet culvert (type 12 - 16)

The results show that given some uncertainty like the representation of ditches and creeks in the topo-bathymetry of the model or the complexity of the in- and outlet structure, numerical results fit fairly well with data, both for the mean water levels and inlet and outlet discharges.

## 8. bottom\_bc

### 8.1 Purpose

This test case is used to validate the boundary conditions on the bed for Telemac-3D simulations

### 8.2 Description of the problem

In this test case two simulations will be run. In `t3d_bottom_inlet.f` a flow rate will be imposed using the boundary conditions on the bed, whereas in `t3d_bottom_source.cas` a source discharge will be imposed on a node on the bed as a source term.

#### 8.2.1 Geometry and Mesh

The configuration of this test case is simple, it is a square box of sides 4000 m. The depth is constant, and initially set to 500 m. The geometry of the test case is shown in figure 8.1.

Furthermore, two different meshes will be used, a fine mesh and a coarse mesh. Since source terms are imposed on a node, the coarse mesh is used to impose the inflow on a single node, and it will be used for `t3d_bottom_source.cas`. Since applying a flow rate can be done on several nodes on the bed, the finer mesh will be compared to the coarse mesh for `t3d_bottom_inlet.cas` simulation results. The coarseness of the mesh is also present for the distribution of the planes in the simulation. The fine mesh has a smaller plane spacing near the bed and the free surface, whereas the coarse mesh has the same number of planes, but these are distributed evenly on the bottom half of the domain and the plane spacing decreases towards the free-surface.

#### 8.2.2 Initial and Boundary Conditions

A discharge  $Q$  of  $10000 \text{ m}^3\text{s}^{-1}$  will be imposed inside a circle with diameter  $D$  of 100 meters placed at the centre of the bed. All vertical boundaries will be defined as walls, see figure 8.1.

#### 8.2.3 Numerical parameters

The key numerical parameters for `t3d_bottom_inlet.f` are:

- OPEN BOUNDARY CONDITIONS ON THE BED = YES
- PRESCRIBED FLOWRATES ON THE BED = 10000.
- NON-HYDROSTATIC VERSION : YES

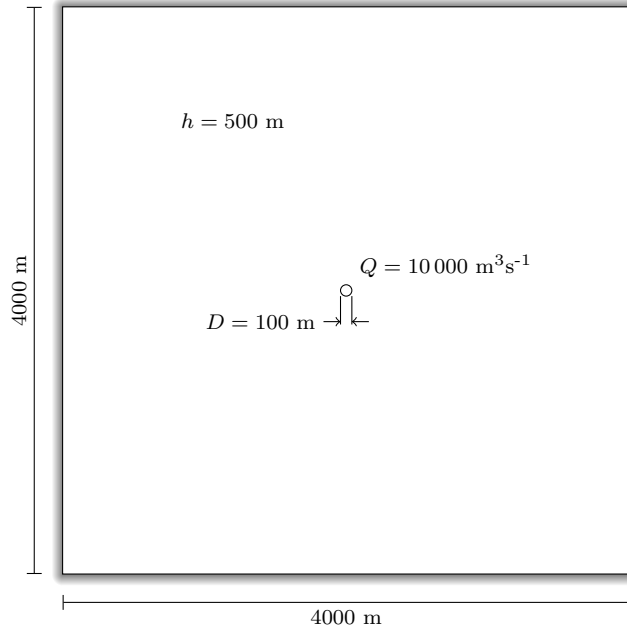


Figure 8.1: Geometrical parameters of the test case.

The key numerical parameters for `t3d_bottom_source.cas` are:

- ABSCISSAE OF SOURCES = 2000.0
- ORDINATES OF SOURCES = 2000.0
- ELEVATIONS OF SOURCES = -500.0
- WATER DISCHARGE OF SOURCES = 10000
- NON-HYDROSTATIC VERSION : YES

### 8.3 Results

At the moment, no post processing is done, however it would be good to have a comparison of the water depth profiles at  $y = 2000 \text{ m}$  and the vertical velocity profiles at  $x = 2000 \text{ m}$  and  $y = 2000 \text{ m}$ . Contour plots of the vertical velocities at  $y = 2000 \text{ m}$  would also be useful.

# 9. bump

## 9.1 Purpose

This test calculates the fluvial regime in a horizontal straight channel including a topographical singularity. This problem has a bidimensionnal analytical solution in 2D. Therefore, it allows testing the accuracy on the computation of the free-surface, with respect to the bottom gradient.

## 9.2 Description

For a given discharge per unit length  $Q$ , imposed at the upstream boundary and a water depth  $H$  imposed at the downstream boundary, the water line fulfils the Bernoulli equations:

$$\frac{Q^2}{2gh^3} + (h + Z_f) = H_0, \quad (9.1)$$

with:

$H_0$  specific energy

$h$  water depth

$Z_f$  bottom elevation

The profile of the singularity is defined by:

$$Z_f = 3 \sin^2 \left( \frac{x - \frac{1}{2}(L - L_0)}{L_0} \right), \quad (9.2)$$

with:

$L$  length of the channel

$L_0$  width of the bump

$x$  abscissa of the point

### 9.2.1 Reference

Hydrodynamics of Free Surface Flows modelling with the finite element method. Jean-Michel Hervouet (Wiley, 2007) pp 128-129.

### 9.2.2 Geometry and Mesh

#### Bathymetry

Flat straight channel with a bump in the centre of the channel (figure 3.6.1)

Bottom of the flat part of the channel at -0.2 m

Height of the bump is 20 cm ( $x = 10$  cm)

### Geometry

Channel length = 20.96 m

Channel width = 2 m (figure 3.6.1)

### Mesh

2,620 triangular elements

1,452 nodes

The mesh is made up of squares whose sides measure 16 cm cut into triangles

5 layers regularly spaced on the vertical (see figure 3.6.1)

### 9.2.3 Physical parameters

Constant horizontal viscosity =  $10^{-6}$  m<sup>2</sup>/s

Vertical turbulence model: mixing length model

Coriolis: no

Wind: no

### 9.2.4 Initial and Boundary Conditions

#### Initial conditions

No velocity

Level of free surface at initial state: 40 cm

#### Boundary conditions

Channel banks: solid boundary without roughness

Bottom: solid boundary with roughness (Strickler = 50 m<sup>1/3</sup>/s)

Upstream imposed discharge 2 m<sup>3</sup>/s

Downstream imposed water level 0.4 m

### 9.2.5 General parameters

Time step 0.01 s

Simulation duration: 50 s

### 9.2.6 Numerical parameters

Non-hydrostatic simulation

Advection of velocities: characteristics

### 9.2.7 Comments

#### 9.3 Results

Qualitatively the velocity field is regular at the surface and vertically in the critical flow area. It follows well the shape of the bump (Figure 3.6.2). Generally, the results are in good agreement with the analytical solution (described in details in [1]). The position of the hydraulic jump is correctly computed. However, a shift (difference of the free surface at the entrance) is observed on the free surface, which seems to be due to the TELEMAC-2D calculus of the free surface used by TELEMAC-3D.

### 9.4 Conclusion

This flow is well reproduced by TELEMAC-3D.

# 10. bump\_static

**10.1 Purpose**

**10.2 Description**

**10.2.1 Reference**

**10.2.2 Geometry and Mesh**

Bathymetry

Geometry

Mesh

**10.2.3 Physical parameters**

**10.2.4 Initial and Boundary Conditions**

Initial conditions

Boundary conditions

**10.2.5 General parameters**

**10.2.6 Numerical parameters**

**10.2.7 Comments**

**10.3 Results**

**10.4 Conclusion**

# 11. canal

## 11.1 Purpose

This study case verifies that TELEMAC-3D is able to compute the free surface evolution along a channel with bottom friction.

## 11.2 Description

The chosen configuration is a straight channel 500 m long and 100 m wide with a flat horizontal bottom (see figure 3.1.1). Three different cases are studied:

- A 2D computation using TELEMAC-2D,
- A 3D computation with hydrostatic option,
- A 3D computation with non-hydrostatic option.

In all cases, the flow establishes a steady flow where the free surface is influenced by the friction on the bottom.

### 11.2.1 Reference

### 11.2.2 Geometry and Mesh

#### Bathymetry

Flat horizontal bottom

#### Geometry

Channel length = 500 m

Channel width = 100 m

#### Mesh

551 triangular elements

319 nodes

10 levels regularly spaced on the vertical. The repartition of the levels is presented on figure 3.1.1

### 11.2.3 Physical parameters

Horizontal constant viscosity:

- no with the hydrostatic option,
- $0.1 \text{ m}^2/\text{s}$  with the non-hydrostatic option

Vertical turbulence model: Nezu and Nakagawa mixing length model

Wind: no

### 11.2.4 Initial and Boundary Conditions

#### Initial conditions

Steady flow (3D cases initialised from the 2D case result file)

#### Boundary conditions

Upstream prescribed flow rate:  $50 \text{ m}^3/\text{s}$

Downstream prescribed elevation: 0.5 m

### 11.2.5 General parameters

Time step: 2 s

Simulation duration: 4,000 s for the 2D computation then 2,000 s more for 3D computations.

### 11.2.6 Numerical parameters

Advection of velocity: Characteristics

### 11.2.7 Comments

#### 11.3 Results

On figure 3.1.2, the 3 free surfaces profiles corresponding to each simulation are compared. These three results are in agreement. We can also observe that the flow is completely symmetrical without any influence of the space discretisation.

### 11.4 Conclusion

TELEMAC-3D is able to take into account correctly the bottom friction term.

## 12. Schematic culvert test case

### 12.1 Purpose

The purpose of this case is to test the culvert functionality in TELEMAC-3D, qualitatively checking that the behaviour of the flow between a tide-controlled river and a floodplain is consistent.

### 12.2 Description

This schematic test case consists of a piece of flood plain and a piece of tidal river from an estuary and they are separated by a dike. There is water exchange between the floodplain and the estuary through two culverts. In normal tidal conditions the tide can enter the floodplain and this will create tidal nature like mud flats and marshes. In storm conditions the culverts are closed and the floodplain is used as a buffer to store water. The crest level of the dike between the estuary and the floodplain is a little lower than the other dikes containing the estuary. When extreme high water levels occur inside the estuary, water can flow over the dike into the floodplain. In this schematic test case we only want to simulate the exchange of water between estuary and floodplain through two culverts.

The floodplain has a bed level of 1m (TAW = Belgian reference level where 0m is about mean low water level). The dike has a crest level of 6m and the estuarine river has a bed level of -5m. An overview of the configuration is given in Figure 12.1. On the right side, the river side, a liquid boundary is set and a tidal signal (i.e. a measured tidal signal from tidal gauge at Schoonaarde, Belgium in the Scheldt estuary) in the form of water levels is applied. Two nodes in the estuary communicate with two nodes in the floodplain to represent the two culverts. One culvert allows flow in both directions and the other culvert only allows flow from the floodplain back to the estuary (this type of culvert in the Scheldt estuary always has a one-way valve and makes sure flood water can return to the estuary after a storm surge).

### 12.3 Computational options

#### 12.3.1 Mesh

#### 12.3.2 Initial and boundary conditions

The water level in the river is prescribed through tidal boundary conditions.

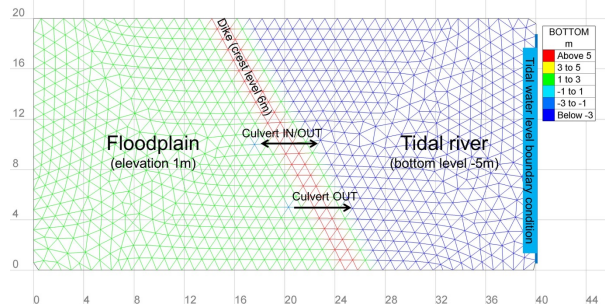


Figure 12.1: Overview of schematic test case for culvert testing

### 12.3.3 Numerical parameters

The simulation time is about 28 hours. The time step is set to 1 second, providing, together with the chosen mesh resolution, a stable simulation.

The bottom friction is taken into account in the model through the Manning Strickler's parameter  $n$ , set to  $0.02 s.m^{-1/3}$ . The horizontal and vertical turbulence viscosity coefficients are both set to  $0.01 m^2 s^{-1}$ .

### 12.3.4 Culvert characteristics

The characteristics of the culverts are presented in Table 12.1.

Table 12.1: Culvert specifications (these are as similar to the real field culverts as possible).

	<b>Culvert 1</b>	<b>Culvert 2</b>
<b>I1</b>	583	637
<b>I2</b>	432	497
<b>CE1</b>	0.5	0.5
<b>CE2</b>	0.5	0.5
<b>CS1</b>	1	1
<b>CS2</b>	1	1
<b>LRGbus</b>	1	2
<b>Haut1</b>	1.9	1.5
<b>CLP</b>	0	2
<b>LBUS</b>	0.2	0.2
<b>z1</b>	4	1.5
<b>z2</b>	4.7	1.5
<b>CV</b>	0	1
<b>C56</b>	10	10
<b>CV5</b>	1.5	1.5
<b>C5</b>	6	6
<b>Ctrash</b>	0.8	0.1
<b>Haut2</b>	1.2	1.5
<b>Fric</b>	0.015	0.015
<b>Length</b>	13	40
<b>circ</b>	0	0

## 12.4 Results

Figure 12.2 shows the results of a short simulation with the schematic scenario. The blue line gives the water level in the estuarine river part and the red line gives the water level in the floodplain. From the characteristics of the two culverts we can see that only culvert 1 allows flow in both directions ( $CLP=0$ ) and the base level of this culvert ( $\max(z1,z2)$ ) is at 4.7m. In Figure 12.2 we see that the flow in the floodplain only starts when the water level in the estuary has reached 4.7m. Because of the small scale of the schematic model and the real life characteristics of the culverts the outflow of water out of the floodplain follows the estuarine water level one on one.

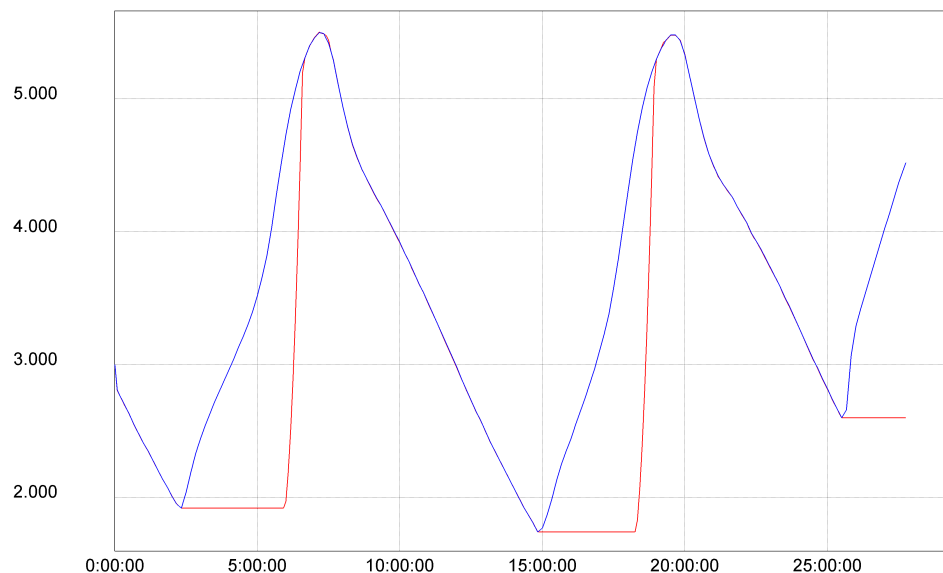


Figure 12.2: Schematic culvert test case : results of two tidal cycles. The blue line gives the water level in the estuarine river part and the red line gives the water level in the floodplain.

# 13. delwaq

## 13.1 Purpose

This test demonstrates the availability of TELEMAC-3D to be chained with DELWAQ, the water quality software from Deltares. This is a one way-chaining by files.

## 13.2 Description

A 20 m wide prismatic channel with trapezoidal cross-section contains bridge-like obstacles in one cross-section made of two abutments and two circular 4 m diameter piles. The flow resulting from steady state boundary conditions is studied. The deepest water depth is 4 m. The hydrodynamic part is similar to the pildepon test case.  
The tracer used is temperature.

### 13.2.1 Reference

### 13.2.2 Geometry and Mesh

#### Bathymetry

Trapezoidal cross section. Maximum water depth = 4 m

#### Geometry

Channel length = 28.5 m

Channel width = 20 m

#### Mesh

4,304 triangular elements

2,280 nodes

6 planes regularly spaced on the vertical (see figure ???)

### 13.2.3 Physical parameters

Vertical turbulence model: mixing length model

Horizontal viscosity for velocity: 0.005 m<sup>2</sup>/s

Coriolis: no

**13.2.4 Initial and Boundary Conditions****Initial conditions**

Constant elevation (= 0 m)

No velocity Uniform temperature at 0

**Boundary conditions**

Upstream: imposed flow rate ( $62 \text{ m}^3/\text{s}$ ) and imposed uniform profile of temperature over the vertical along a segment equal to 1

Downstream: prescribed elevation ( = 0 = initial elevation)

**13.2.5 General parameters**

Time step: 0.1 s

Simulation duration: 5 s

**13.2.6 Numerical parameters**

Non-hydrostatic version

Advection for velocities and tracer: Characteristics method

**13.2.7 Comments****13.3 Results**

If running DELWAQ with the DELWAQ result files written by TELEMAC-3D, the velocity results are similar with both codes.

**13.4 Conclusion**

TELEMAC-3D can be used to chain with DELWAQ.

# 14. gouttedo

## 14.1 Purpose

This test demonstrates that the TELEMAC-3D solution is not polarised because it can simulate the circular spreading of a wave in a square domain. It also shows that the no-flow condition is satisfied on solid boundaries and that the solution remains symmetric after reflection of the circular wave on the boundaries.

## 14.2 Description

The fluid is initially at rest with a Gaussian free surface in the centre of a square domain (see figure 3.3.2). The evolution of the surface and the reflection of the wave by the solid boundaries are then calculated during 4 seconds.

### 14.2.1 Reference

### 14.2.2 Geometry and Mesh

#### Bathymetry

Flat bottom

#### Geometry

Square length = 20.1 m

#### Mesh

8,978 triangular elements

4,624 nodes

Vertical Mesh: 3 planes regularly spaced on the vertical (see figure 3.3.1)

### 14.2.3 Physical parameters

Turbulence: constant viscosity in both directions (molecular viscosity)

Bottom friction: Chézy law with coefficient equal to  $60 \text{ m}^{1/2}/\text{s}$

Coriolis: no

Wind: no

#### 14.2.4 Initial and Boundary Conditions

##### Initial conditions

Water depth at boundary: 2.4 m

Water depth at the centre: 4.8 m

No velocity

##### Boundary conditions

Solid wall with slip condition

#### 14.2.5 General parameters

Time step: 0.04 s

Simulation duration: 4 s

#### 14.2.6 Numerical parameters

Non-hydrostatic computation

Advection for velocities: PSI-type MURD scheme

#### 14.2.7 Comments

The initial free surface elevation is prescribed in the CONDIM subroutine.

### 14.3 Results

The wave spreads circularly around the initial water surface peak elevation (Figure 3.3.2 to Figure 3.3.4). When it reaches the boundaries, reflection occurs. The reflected wave is also axi-symmetric. The final volume in the domain is equal to the initial volume.

### 14.4 Conclusion

Even though the mesh is polarised (along the  $x$  and  $y$  directions and the main diagonal), the solution is not. Solid boundaries are treated properly: no bias occurs in the reflected wave. Water mass is conserved.

# 15. Lock-exchange

## 15.1 Purpose

This test demonstrates the ability of TELEMAC-3D to model the motion of two fluids with different densities.

## 15.2 Description

This validation case consists of a lock-exchange flow in a rectangular cavity of height  $L$  and length  $7.5L$ . The width of the cavity is equal to  $0.3L$ . The flow consists of fresh water (on the right) and saline water (on the left) separated at  $t = 0$  and suddenly released. The heavy fluid sinks below the lighter one by forming a saline wedge which, according to the observations, makes an angle of about  $\pi/3$  with the bottom [3]. For this test-case, the dimensionless time is defined by:

$$t^+ = \frac{tU}{L} \quad (15.1)$$

with:

$$U = \sqrt{|\beta| S g L} \quad (15.2)$$

Where  $S$  is the salinity in the left-side of the cavity at  $t = 0$  and  $\beta$  the coefficient of haline dilatation.  $U$  is an estimation of the front velocity. Considering that the whole potential energy of the initial conditions is transformed into kinetic energy, it can be estimated that the front velocity is equal to  $0.5U$ . Measurements actually show that the velocity of the lower front is about equal to  $0.47U$ , while that of the upper front is about equal to  $0.59U$  for a free-surface lock exchange flow [2]. The dimensionless numbers describing the flow are the Grashof number and the Schmidt number, defined by:

$$Gr = \frac{U^2 L^2}{\nu^2} \quad (15.3)$$

and:

$$Sc = \frac{\nu}{K} \quad (15.4)$$

where  $\nu$  is the molecular dynamic viscosity and  $K$  is the molecular haline diffusion coefficient. The density law depending on salinity used in TELEMAC-3D reads:

$$\rho = \rho_0(1 + 750.10^{-6}S), \text{ with } \rho_0 = 999.972 \text{ kg/m}^3 \quad (15.5)$$

so that  $\beta$  is equal to  $-7.5.10^{-4} (\text{g/L})^{-1}$ .

### 15.3 Preamble – an attempt at reproducing Adduce *et al.*'s experiments

In order to compare the shape of the simulated flow to experimental results, we first considered the case studied experimentally by Adduce *et al.* [1]. At  $t^+ = 0$ , the separation between the fresh and saline water is now located at  $L$  from the left side of the cavity. The Schmidt number is still equal to 1 but the Grashof number is now equal to  $7.3 \cdot 10^8$  (the salinity is set to 9 g/L in the left part and 0 g/L on the right part, the molecular dynamic viscosity is set to  $2.7 \cdot 10^{-5} m^2 s^{-1}$ ). The non-hydrostatic version of TELEMAC-3D was used, using an N advection scheme with the option 2 and 5 corrections. The dynamic pressure is calculated before the resolution of the wave equation and no turbulence model is used. The figure 15.1 shows the results obtained at  $t^+ = 7.3$  and  $16.4$  compared to the experiments. The velocity of the front seems correctly reproduced by the numerical model, but the shape of the flow is quite different from the experimental one. The simulation was run without using any turbulence model, which may explain why there is less diffusion than in the experiment.

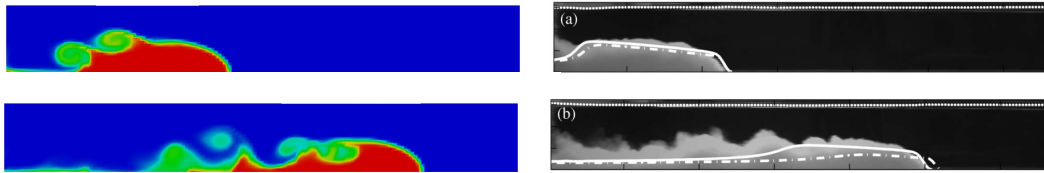


Figure 15.1: Lock-exchange: comparison of the experimental results by Adduce *et al.* [1] (right) at  $t^+ = 7.3$  and  $16.4$  with the simulation results (left), using a N advection scheme with the option 2 and 5 corrections. The dynamic pressure is calculated before the resolution of the wave equation.

The same simulation was then run with the  $k - \epsilon$  turbulence model applied in all directions, but there is no visible impact on the results because this is a case of transition between a laminar and a turbulent flow. In these conditions, it is hard to compare the various advection schemes or numerical options on this case: different flow shapes are obtained but there is never enough diffusion to match the turbulent diffusion observed in the experiments. We did not find reference data regarding a less turbulent experimental setup where the shape of the free-surface flow is displayed. Thus, we chose to simulate a case without available experimental data but with a lower Grashof number.

### 15.4 Case setup

#### 15.4.1 Geometry and mesh

Given the difficulties in reproducing a free-surface experimental setup, the case simulated here is the one described in J. Jankowski's PhD thesis [4]. The flow consists of fresh water (on the right) and saline water (on the left) separated at  $t^+ = 0$  at the half-width of the domain. The Schmidt number is equal to 1 and the Grashof number is equal to  $8 \cdot 10^7$  (the salinity is set to 1 g/L in the left part and 0 g/L on the right part, the molecular dynamic viscosity is set to  $2.7 \cdot 10^{-5} m^2 s^{-1}$ ).

#### Bathymetry

The bed of the cavity is flat at the elevation  $z = -4$  m.

### Geometry

The cavity is 30 m long and 1.2 m wide.

### Mesh

The mesh consists of 1,806 triangular elements, which corresponds to 1,060 nodes. Along the vertical, 24 regularly spaced planes are used. The figure 15.2 shows a vertical and a horizontal section of the mesh.



Figure 15.2: Lock-exchange: vertical (top) and a horizontal (bottom) sections of the mesh.

### 15.4.2 Physical parameters

The influence of the Coriolis force and meteorological forcings are not taken into account.

### 15.4.3 Initial and Boundary Conditions

#### Initial conditions

- Constant water depth = 4 m
- No velocity
- Initial salinity: 1 g/L on the left half part and 0 g/L in the other part (defined in the subroutine **T3D\_CONDIM** and the keyword **INITIAL VALUES OF TRACERS**) – see the figure 15.3.

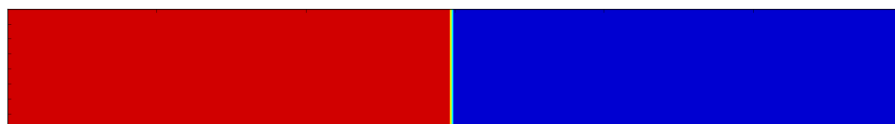


Figure 15.3: Lock-exchange: initial salinity distribution, ranging from 0 (blue) to 1 (red).

#### Boundary conditions

- Closed boundaries
- No bottom friction

### 15.4.4 General parameters

- Time step: 0.5 s
- Simulation duration: 100 s

### 15.4.5 Numerical parameters

- Advection of velocities and tracers: tests with the characteristics scheme, SUPG, the Leo-Postma scheme and the N and PSI-type MURD schemes with options 1, 2 and 3 and several numbers of corrections
- DYNAMIC PRESSURE IN WAVE EQUATION: runs with this key-word set to YES and NO (dynamic pressure calculated before and after the wave equation resolution, respectively)

- Linear solver: solver 7 (GMRES) used with a precision of  $10^{-10}$  and a maximum of 2000 iterations for all the matrix inversions
- Implicitation coefficients on the velocity and depth : 0.5
- Non-hydrostatic version: used to test the advection schemes and dynamic pressure option, one hydrostatic run also performed to compare to the non-hydrostatic version

## 15.5 Reference results

There is no available experimental data regarding the shape of the flow for this specific case, but we have an estimation of the angle between the wedge and the bottom and the front velocity values. The angle should be about equal to  $\pi/3$  and the lower front velocity should be about equal to 0.081m/s. On this case, it is also expected that Rayleigh-Taylor instability cells will form at the interface between the two fluids. In order to have an idea what these instabilities should look like, fine simulations were run with the second order predictor-corrector PSI MURD-type advection scheme (the most accurate advection solver in TELEMAC-3D at the moment – SCHEME OPTION FOR THE ADVECTION 3). The triangle size in the horizontal mesh is 0.025m and 80 planes are used, so that the horizontal and vertical discretisations are equal. The 3D mesh contains about 9 million points. The time step size is equal to 0.2 s and the simulation duration is 100 s ( $t^+ = 4.29$ ). The figures 15.4 and 15.5 show the results at  $t^+ = 4.29$  when using 5, 10 and 15 corrections, calculating the dynamic pressure after or before the resolution of the wave equation. We observed that this option has a visible influence on the results.

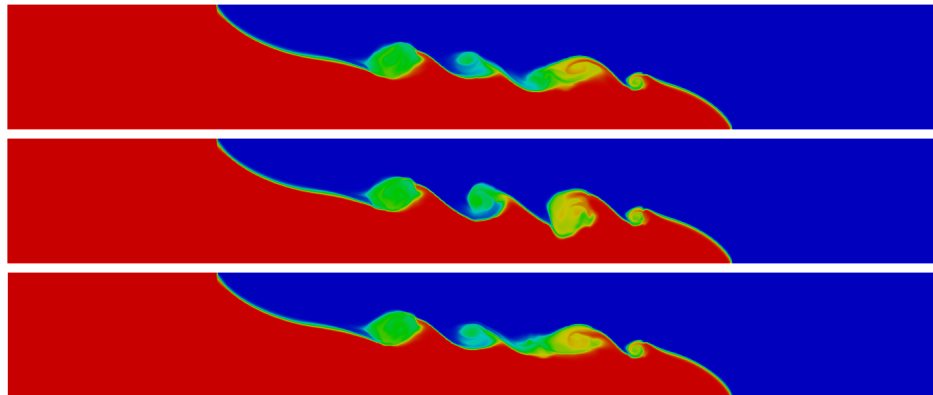


Figure 15.4: Lock-exchange: fine simulation results at  $t^+ = 4.29$  with a PSI advection scheme with the option 3, using 5, 10 and 15 corrections (from top to bottom). The dynamic pressure is calculated after the resolution of the wave equation.

The mean velocity of the lower front is equal to 0.084 m/s and the angle between the wedge front and the vertical is about equal to  $\pi/3$ , which matches experimental observations on this type of flows. It is also visible that several instability cells appear in the simulations. At least three cells appear at the interface, and one or two more depending on the numerical options. The shape of the instability cells is influenced by the option DYNAMIC PRESSURE IN WAVE EQUATION and by the number of corrections in the distributive scheme. These results show that this case is very sensitive to slight numerical changes. In what follows, we will compare the various advection schemes, the DYNAMIC PRESSURE IN WAVE EQUATION option and the hydrostatic version of TELEMAC-3D on this case: for a given discretisation, we will observe whether the main instability cells appear or not, and check the value of the angle to the bottom

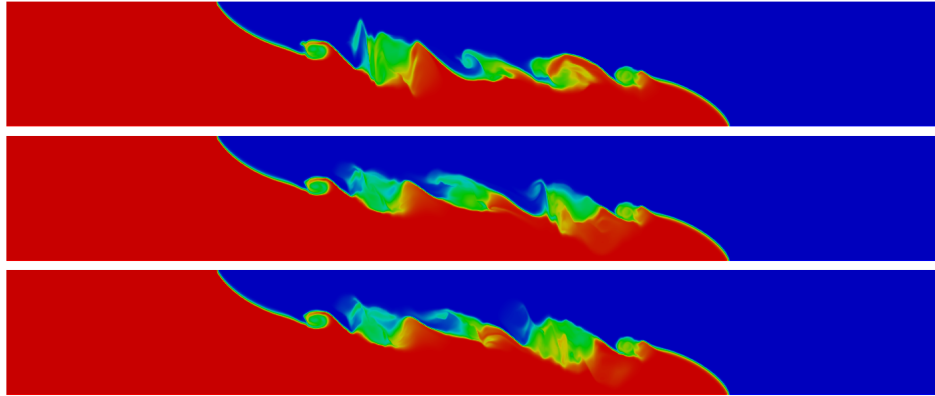


Figure 15.5: Lock-exchange: fine simulation results at  $t^+ = 4.29$  with a PSI advection scheme with the option 3, using 5, 10 and 15 corrections (from top to bottom). The dynamic pressure is calculated before the resolution of the wave equation.

and of the front velocity.

## 15.6 Results

### 15.6.1 Dynamic pressure not included in the wave equation

#### Characteristics

The figure 15.6 shows the results obtained with the characteristics advection scheme at  $t^+ = 4.29$ . The lower front velocity is equal to 0.072m/s in the simulation (as compared to 0.081m/s) and the angle of the wedge is well captured by the model but it is so diffusive that the Rayleigh-Taylor instabilities do not trigger.

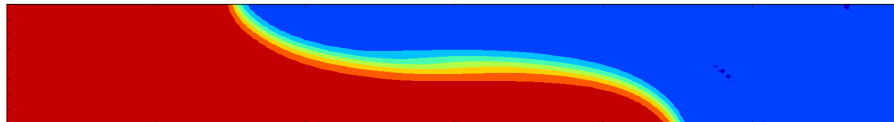


Figure 15.6: Lock-exchange: simulation result at  $t^+ = 4.29$  with the characteristics advection scheme. The dynamic pressure is calculated after the resolution of the wave equation.

#### SUPG

The figure 15.7 shows the results obtained with the SUPG advection scheme, with the option 2 on the velocity and tracer and the option 0 on the water depth, at  $t^+ = 4.29$ . It is visible that the maximum principle is not fulfilled with this scheme since the final tracer values are outside the initial bounds. The spurious behaviour mostly occurs at the upper and lower fronts, in the white zones of the plot. On the other hand, the lower front velocity is equal to 0.082m/s in the simulation (as compared to 0.081m/s) and the angle of the wedge is well captured by the model. It is however too diffusive to let instabilities develop during the simulation. They are slightly visible in the results, but still very diffused.

#### Leo Postma scheme

The figure 15.8 shows the results obtained with the Leo Postma advection scheme at  $t^+ = 4.29$ . The lower front velocity is equal to 0.074m/s in the simulation (as compared to 0.081m/s) and

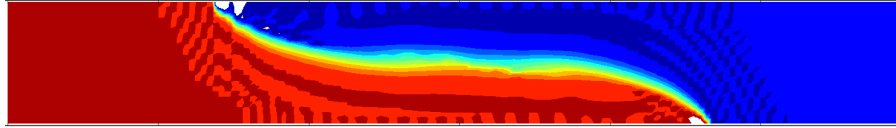


Figure 15.7: Lock-exchange: simulation result at  $t^+ = 4.29$  with the SUPG advection scheme with the salinity ranging from -0.1 (dark blue) to 1.1 (dark red) on the top and from -1.4 (blue) to 2 (red) on the bottom. The dynamic pressure is calculated after the resolution of the wave equation.

the angle of the wedge is well captured by the model. The model but it is too diffusive, so that the Rayleigh-Taylor instabilities do not trigger in the simulation.

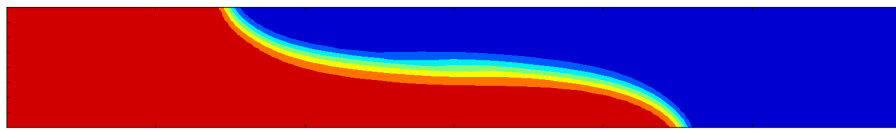


Figure 15.8: Lock-exchange: simulation result at  $t^+ = 4.29$  with the Leo Postma advection scheme. The dynamic pressure is calculated after the resolution of the wave equation.

### PSI (or N) scheme

The figures 15.9 to 15.11 show the results obtained with the options 1, 2 and 3 with the PSI scheme, using two to five corrections, at  $t^+ = 4.29$ . We recall that the option 1 corresponds to the classical scheme, the option 2 is the first order predictor-corrector scheme and the option 3 is the second-order predictor corrector scheme. The results obtained with the N scheme are very similar so they are not shown here. It appears in the results that for this discretisation the first order predictor-corrector scheme provides better results than the second-order one since they present more instability cells. Both have converged after about 4 corrections. The lower front velocity is equal to ??m/s in the simulations (as compared to 0.081m/s).

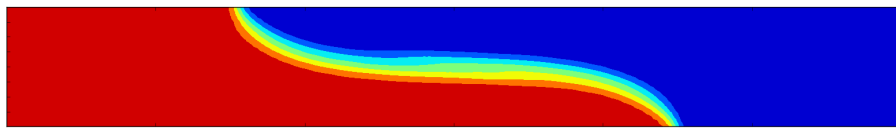


Figure 15.9: Lock-exchange: simulation result at  $t^+ = 4.29$  with a PSI advection scheme with the option 1. The dynamic pressure is calculated after the resolution of the wave equation.

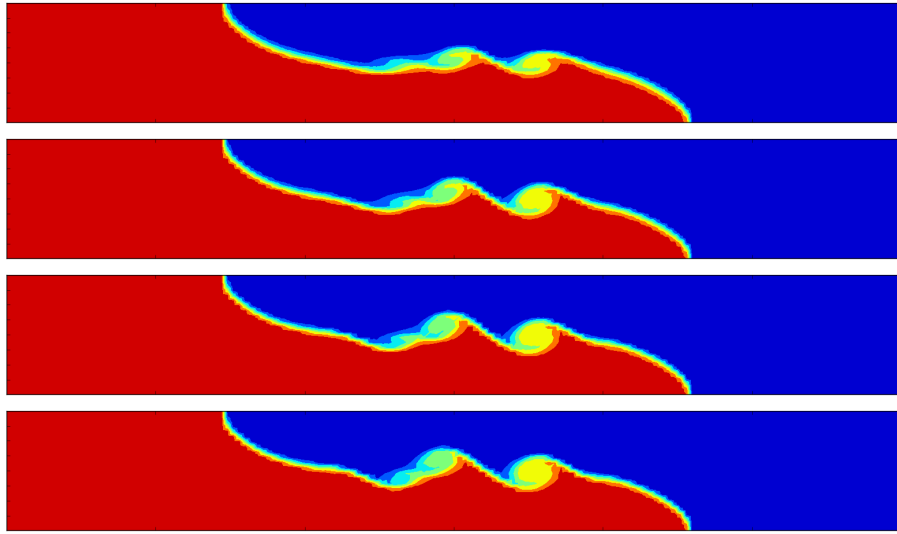


Figure 15.10: Lock-exchange: simulation result at  $t^+ = 4.29$  with a PSI advection scheme with the option 2, using 2, 3, 4 and 5 corrections (from top to bottom). The dynamic pressure is calculated after the resolution of the wave equation.

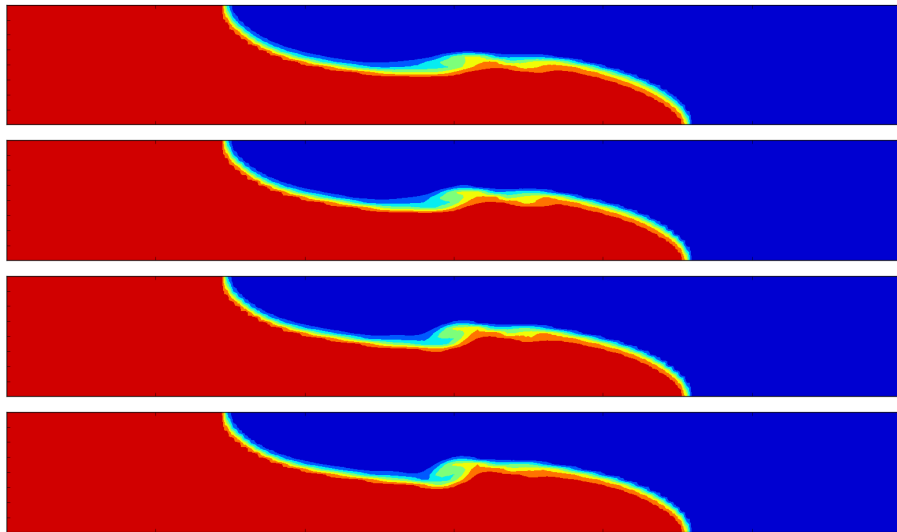


Figure 15.11: Lock-exchange: simulation result at  $t^+ = 4.29$  with a PSI advection scheme with the option 3, using 2, 3, 4 and 5 corrections (from top to bottom). The dynamic pressure is calculated after the resolution of the wave equation.

### 15.6.2 Dynamic pressure included in the wave equation

In this section we show the results obtained when the dynamic pressure is calculated before the resolution of the wave equation (thus, before the hydrostatic pressure). This change does not impact the results obtained with the characteristics, SUPG and Leo Postma schemes because they are so diffusive that for this discretisation the instability cells do not appear. However, the results obtained with the predictor-corrector PSI scheme are influenced by this option. The same holds for the N scheme, but once again the results obtained with the N and PSI schemes were so close that we chose to show only the results of the PSI scheme, which were even slightly improved compared to the results of the N scheme. Here we only show the results obtained with the first-order predictor-corrector PSI scheme since we saw previously that it provides the best results for this mesh discretisation.

#### PSI scheme

The figure 15.12 shows the results obtained with the option 2 for the PSI scheme, using two to five corrections, at  $t^+ = 4.29$ .

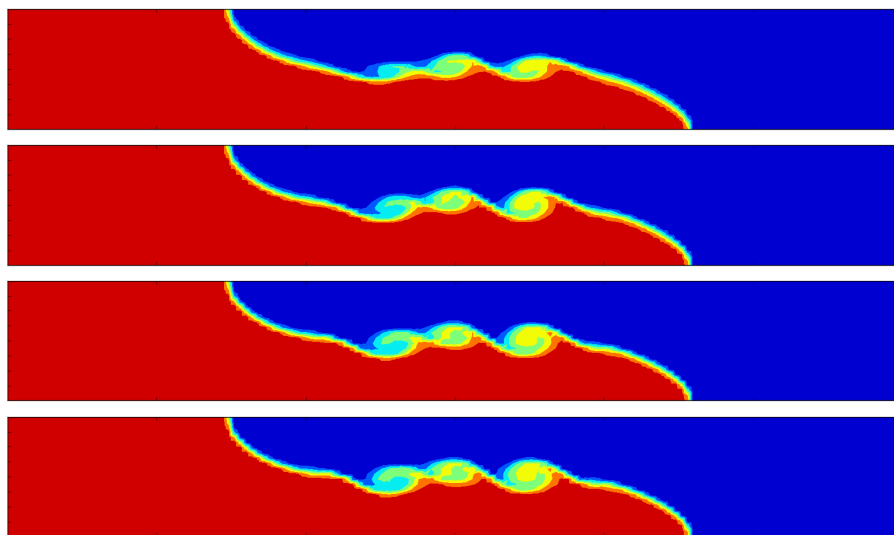


Figure 15.12: Lock-exchange: simulation result at  $t^+ = 4.29$  with a PSI advection scheme with the option 2, using 2, 3, 4 and 5 corrections (from top to bottom). The dynamic pressure is calculated before the resolution of the wave equation.

### 15.6.3 Hydrostatic hypothesis

The results of the hydrostatic computation are presented in the figure 15.13. The average velocity of the lower front is approximately 0.068 m/s and the angle of the wedge compared to the bottom is close to 90°. Besides, the instability cells do not appear in the results. This shows that the hydrostatic hypothesis is not valid for this type of case.

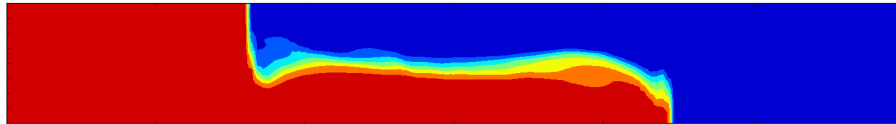


Figure 15.13: Lock exchange test: results with the hydrostatic hypothesis

## 15.7 Conclusion

In this document, a sensitivity analysis on the lock-exchange case was performed. First, we tried to reproduce an experimental setup, but realized we could not correctly reproduce the flow shape with TELEMAC-3D: without a turbulence closure, there is not enough diffusion in the numerical result whereas using the  $k - \varepsilon$  turbulence model is way too diffusive. Thus, we chose a less turbulent setup, which is actually the one proposed in J. Jankowski's PhD thesis and was already used as a TELEMAC-3D example. We used twice as many planes as in the original simulation, using the non-hydrostatic version of TELEMAC-3D and testing the various advection schemes and the option DYNAMIC PRESSURE IN WAVE EQUATION. We also compared the hydrostatic and non-hydrostatic versions. In order to have a reference solution, fine simulations for this case were run, with a space discretisation of 0.025m (9 million points in 3D). The results of the fine simulations showed that Rayleigh-Taylor instabilities appear at the interface between the two fluids. There are three major central cells and, depending on the options, one or two smaller external cells. Their shape is influenced by the number of corrections used in the distributive scheme and the choice for the option DYNAMIC PRESSURE IN WAVE EQUATION.

In the coarser simulations, we observed that only the N or PSI MURD-type advection schemes with the option 2 (1st order predictor-corrector) or 3 (2nd order predictor-corrector) are accurate enough to reproduce the instability cells with this discretisation (0,2m). The 2nd order predictor-corrector PSI or N schemes have a higher order of convergence than the 1st order one, but for this discretisation the latter provide better results. The three main instability cells only appear when setting the option DYNAMIC PRESSURE IN WAVE EQUATION to YES and with the 1st order predictor-corrector N or PSI schemes. The results thus seem to be improved by calculating the dynamic pressure before the resolution of the wave equation. We can also conclude that the options 2 or 3 for the MURD-type advection schemes greatly improve the quality of the numerical solution provided by TELEMAC-3D compared to all the other advection schemes. However, it seems difficult for the user to choose the number of corrections to apply in the distributive schemes and a possible improvement would be to let TELEMAC-3D decide when the algorithm has converged based on a convergence criterion.

On the other hand, the results show that the hydrostatic hypothesis is not valid for this type of case: the shape of the flow is not correctly reproduced with the hydrostatic option.

Finally, it is important to keep in mind that this test-case is very sensitive due to its unstable

nature, and that slight changes to the schemes might lead to significant differences when it comes to the shape of the instabilities.

# 16. malpasset

## 16.1 Purpose

This test illustrates that TELEMAC-3D is able to simulate a real dam break flow on an initially dry domain. It also shows the propagation of the wave front and the evolution in time of the water surface and velocities in the valley downstream.

## 16.2 Description

This case is the simulation of the propagation of the wave following the break of the Malpasset dam (South-East of France). Such accident really occurred in December 1959. The model represents the reservoir upstream from the dam and the valley and flood plain downstream. The entire valley is approximately 18 km long and between 200 m (valley) and 7 km wide (flood plain). The complete study is described in details in [1]. The simulation is performed using 2 or 6 vertical planes ("pos\_p2" and "pos\_p6") using the treatment of negative depths introduced since TELEMAC-3D 7.0. The historical simulation using 2 vertical planes and the method of characteristics (named "charac\_p2") has been kept. Nevertheless, the recommended advection scheme for velocities for such applications is now the N-type MURD scheme (14). A simulation using 2 vertical planes with a large mesh (named "large") is also performed.

### 16.2.1 Reference

[1] Hydrodynamics of Free Surface Flows modelling with the finite element method. Jean-Michel Hervouet (Wiley, 2007) pp. 281-288.

### 16.2.2 Geometry and Mesh

#### Bathymetry

Real topography

#### Geometry

Size of the model domain  $\approx 17 \text{ km} \times 9 \text{ km}$

#### Mesh

The mesh is refined in the river valley (downstream from the dam) and on the banks.

Regular mesh: 26,000 triangular elements / 13,541 nodes. Maximum size range is from 17 to 313 m

Large mesh: 104,000 triangular elements / 53,081 nodes. Maximum size range is from 8.5 to

156.5 m

2 or 6 layers regularly spaced on the vertical

### 16.2.3 Physical parameters

Constant viscosity equal to  $0.1 \text{ m}^2/\text{s}$  on vertical and horizontal directions

Coriolis: no

Wind: no

### 16.2.4 Initial and Boundary Conditions

#### Initial conditions

Full reservoir at initial time

No water in the downstream valley

No velocity

#### Boundary conditions

Channel banks: solid boundary without roughness (slip conditions)

Bottom: solid boundary with roughness. Strickler formula with friction coefficient =  $30 \text{ m}^{1/3}/\text{s}$

Solid boundary everywhere

### 16.2.5 General parameters

Time step: 4 s for regular mesh cases and 1 s for large mesh case

Simulation duration: 4,000 s

### 16.2.6 Numerical parameters

Non-hydrostatic simulation

Advection of velocities: N-type MURD scheme for tidal flats with the treatment of negative depths for three cases (regular mesh with 2 or 6 planes + large mesh), the method of characteristics for the 4<sup>th</sup> one.

### 16.2.7 Comments

## 16.3 Results

Figure ??? illustrates the progression of the flood wave after the dam break (simulation using the treatment of negative depths that smoothes the results on tidal flats). The propagation of the wave front is very fast. The water depths increase rapidly in the valley downstream from the dam location. The wave spreads in the plain when arriving to the sea. During the simulation, no negative water depths are observed. Figure ??? presents the water depth at time = 400 s obtained with 2 planes (p2), 6 planes (p6) and the treatment of negative depths, 2 planes using the method of characteristics (charac) and 2 planes using the fine mesh (p2\_large) calculations. The results are similar.

## 16.4 Conclusion

TELEMAC-3D is capable of simulating the propagation of a dam break wave in a river valley initially dry.

# 17. particles

## 17.1 Purpose

This test demonstrates the ability of TELEMAC-3D to track the transport of particles which are released into the fluid from discharge points.

## 17.2 Description

### 17.2.1 Reference

### 17.2.2 Geometry and Mesh

**Bathymetry**

**Geometry**

**Mesh**

3,780 triangular elements

2,039 nodes

10 planes regularly spaced on the vertical

### 17.2.3 Physical parameters

Vertical turbulence model: mixing length model

Horizontal viscosity for velocity: 0.01 m<sup>2</sup>/s

Coriolis: no

### 17.2.4 Initial and Boundary Conditions

**Initial conditions**

Initialisation from a 2D result file (water depth and horizontal velocity components).

**Boundary conditions**

Upstream: imposed flow rate (700 m<sup>3</sup>/s)

Downstream: prescribed elevation (= 265 m)

### 17.2.5 General parameters

Time step: 5 s

Simulation duration: 7200 s = 2 h

Number of released particles: 100

**17.2.6 Numerical parameters**

Non-hydrostatic version

Advection for velocities and tracer: Characteristics method

**17.2.7 Comments****17.3 Results****17.4 Conclusion**

# 18. pildepon

## 18.1 Purpose

This test demonstrates the availability of TELEMAC-3D to represent the impact of an obstacle on a channel flow. It also demonstrates the capability to represent unsteady eddies in a model with steady state boundary.

## 18.2 Description

A 20 m wide prismatic channel with trapezoidal cross-section contains bridge-like obstacles in one cross-section made of two abutments and two circular 4 m diameter piles. The flow resulting from steady state boundary conditions is studied. The deepest water depth is 4 m.

### 18.2.1 Reference

### 18.2.2 Geometry and Mesh

#### Bathymetry

Trapezoidal cross section. Maximum water depth = 4 m

#### Geometry

Channel length = 28.5 m

Channel width = 20 m

#### Mesh

4,304 triangular elements

2,280 nodes

6 planes regularly spaced on the vertical (see figure 3.5.1)

### 18.2.3 Physical parameters

Vertical turbulence model: mixing length model

Horizontal viscosity for velocity: 0.005 m<sup>2</sup>/s

Coriolis: no

### 18.2.4 Initial and Boundary Conditions

#### Initial conditions

Constant elevation (= 0 m)

No velocity

**Boundary conditions**

Upstream: imposed flow rate ( $62 \text{ m}^3/\text{s}$ )

Downstream: prescribed elevation ( $= 0$  = initial elevation)

**18.2.5 General parameters**

Time step: 0.1 s for the hydrostatic version, 0.4 s for the non-hydrostatic version

Simulation duration: 80 s

**18.2.6 Numerical parameters**

Hydrostatic and non-hydrostatic computation

Advection for velocities: Characteristics method

**18.2.7 Comments****18.3 Results**

The obstacles create a contraction of the streamlines, and Karman vortices are observed behind the piers. The Karman vortices produce an asymmetry of the velocity field. This velocity field is unsteady behind the piers in the Karman vortices (see top of Figures 3.5.2 and 3.5.3, where depth-averaged velocities are shown for the hydrostatic and non-hydrostatic simulations respectively). On the bottom of the same figure a time profile of the depth-averaged vertical velocity is given. After a transition of about 150 s a periodic regime takes place. Streamlines for positions where  $x > -0.5 \text{ m}$  (behind the piles) are shown of figure 3.5.4 for the hydrostatic (a) and non-hydrostatic (b) simulations. The figures show that the Karman vortices are better represented by the non-hydrostatic simulation, indicating the necessity to solve such turbulence problems using the non-hydrostatic version of TELEMAC-3D.

**18.4 Conclusion**

TELEMAC-3D can be used to study the hydrodynamic impact of engineering works (like bridge piers), and to analyse unsteady flow, such as the Karman vortices.

# 19. plage

## 19.1 Purpose

$k - \omega$  model

## 19.2 Description

### 19.2.1 Reference

### 19.2.2 Geometry and Mesh

#### Bathymetry

A flat channel ( $z = -0.43$  m) with a kind of cavity where the bathymetry is increasing from -0.43 m to 0 m (see Figure ???).

#### Geometry

Flat bottom in the channel part ( $z = -0.43$  m).

Increasing bathymetry -0.43 m to 0 m in the of cavity.

#### Mesh

8,796 triangular elements

4,561 nodes

7 planes regularly spaced on the vertical

### 19.2.3 Physical parameters

Turbulence model:  $k - \omega$  model

Coriolis: no

### 19.2.4 Initial and Boundary Conditions

#### Initial conditions

Constant elevation (= 0.1 m)

No velocity

#### Boundary conditions

Upstream: imposed flow rate ( $0.155 \text{ m}^3/\text{s}$ )

Downstream: prescribed elevation (= 0.1 m = initial elevation)

**19.2.5 General parameters**

Time step: 0.2 s

Simulation duration: 200 s

**19.2.6 Numerical parameters**

Hydrostatic version

Advection for velocities: Characteristics method

**19.2.7 Comments****19.3 Results**

Validation of the  $k - \omega$  turbulence model?

**19.4 Conclusion**

# 20. pluie

## 20.1 Purpose

This test illustrates that TELEMAC-3D is able simulating a rain fall (addition of fresh water on the surface).

## 20.2 Description

We consider a square basin with a water depth of 10 m. The domain is initially at rest with a constant initial salinity equal to 32 g/L.

A fictive rain of 864,000 mm per day (10 mm/s) is simulated during 3 s.

### 20.2.1 Reference

### 20.2.2 Geometry and Mesh

#### Bathymetry

Flat bottom

#### Geometry

Size of the basin domain = 10 m x 10 m (see figure 3.9.1)

#### Mesh

272 triangular elements

159 nodes

21 layers regularly spaced on the vertical

### 20.2.3 Physical parameters

Constant horizontal viscosity equal to 0.1 m<sup>2</sup>/s

Mixing length on the vertical (Nezu-Nakagawa)

Coriolis: no

Wind: no

Rain: 864,000 mm/day (i.e. 10 mm/s)

### 20.2.4 Initial and Boundary Conditions

#### Initial conditions

No velocity

Constant water depth equal to 10 m

Salinity equal to 32 g/L

#### **Boundary conditions**

Solid boundary everywhere

#### **20.2.5 General parameters**

Time step: 1 s

Simulation duration: 3 s

#### **20.2.6 Numerical parameters**

Hydrostatic simulation

Advection of velocities: Characteristics

Advection of tracers: PSI-type MURD scheme

#### **20.2.7 Comments**

### **20.3 Results**

The water mass balance is perfect (of the order of  $10^{-12}$ ). The initial amount of water is 1,000 m<sup>3</sup>. The quantity of rain during the total simulation is 30 mm. Taking into account the surface of the basin (100 m<sup>2</sup>), the quantity of supplied fresh water is equal to 3 m<sup>3</sup>. The log file of the simulation indicates a final mass equal to 1,003 m<sup>3</sup>. In addition, the total tracer (salinity) remains constant (of the order of  $10^{-8}$ ).

Due to the rain, the salinity at the surface decreases during the simulation (see figure 3.9.2). The salinity profile on the vertical at the end of the simulation is presented on figure 3.9.2.

### **20.4 Conclusion**

TELEMAC-3D is capable of simulating the supply of water on the free surface due to the rain.

# 21. Solitary wave

## 21.1 Purpose

This test demonstrates the ability of TELEMAC-3D to model the propagation of a solitary wave with only 2, 3 or 4 vertical levels. In an ideal case, the wave should travel without changing its shape and amplitude. This study demonstrates the necessity of using the non-hydrostatic version of the software to simulate non-linear waves propagation.

## 21.2 Notations

This test-case is the same as described in [4]. The notations are illustrated in the Figure 21.1.

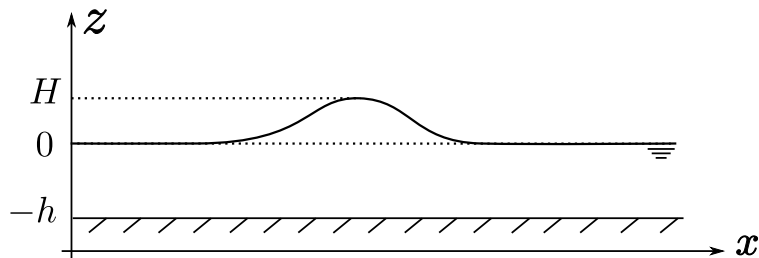


Figure 21.1: Solitary wave propagation over a flat bottom: description of the notations.

## 21.3 Theory

### Authorship

The following description is extracted from the PhD thesis of Jacek A. Jankowski [4]. Only slight changes were done to the text.

A solitary wave is a single elevation of the water surface above an undisturbed surrounding, which is neither preceded nor followed by any free surface disturbances. Neglecting dissipation, as well as bottom and lateral boundary shear, a solitary wave travels over a horizontal bottom without changing its shape and velocity. The accuracy of the model can be evaluated by comparing the amplitude and celerity of the wave with its theoretical values, as well as the

deformation of the wave as it travels.

There are several theories that aim at giving an approximation of the free-surface and velocity field for this form of non-linear finite-amplitude wave. The most known ones are the Stokes and cnoidal waves theories. The latter is used here, based on Laitone [5]. According to [4], it is the most frequently used for comparative studies. It provides approximate formulae for the velocity components  $u, w$ , free surface elevation  $\eta$  defined as  $\eta = z + h$ , pressure  $p$  and wave celerity  $c$  of a solitary wave with a height of  $H$ , on a vertical section of an infinitely long channel of an undisturbed depth  $h$  ( $z = 0$  at the free-surface, see the Figure 21.1). They read:

$$\left\{ \begin{array}{l} u = \sqrt{gh} \frac{H}{h} \operatorname{sech}^2 \left[ \sqrt{\frac{3}{4} \frac{H}{h^3}} (x - ct) \right] \\ w = \left( \sqrt{3gh} \sqrt{\frac{H}{h^3}} \frac{z+h}{h} \right) \operatorname{sech}^2 \left[ \sqrt{\frac{3}{4} \frac{H}{h^3}} (x - ct) \right] \tanh \left[ \sqrt{\frac{3}{4} \frac{H}{h^3}} (x - ct) \right] \\ \eta = h + H \operatorname{sech}^2 \left[ \sqrt{\frac{3}{4} \frac{H}{h^3}} (x - ct) \right] \\ p = \rho g (\eta + z) \\ c = \sqrt{g(H+h)} \end{array} \right. \quad (21.1)$$

It is interesting that in this analytical approximation the vertical velocity component is not treated as small, as commonly taken, but the pressure can be assumed hydrostatic (fourth line of (21.1)) at the same level of exactness as the horizontal velocity (with  $\mathcal{O}((H/h)^2)$ )[5]. Therefore, this initial condition is suitable for fair comparisons between models with and without hydrostatic approximation and the initial value of zero hydrodynamic pressure is assumed. Although the initial velocity field (first two lines of (21.1)) is perfectly divergence-free, larger values of the hydrodynamic pressure appear immediately after the first time step (60% of the value of the hydrostatic pressure at the bottom).

Following the test cases provided by Ramaswamy [6], a solitary wave described by (21.1) is applied in a long channel as an initial condition, and the behaviour of the solution is observed thereafter. Due to the fact that the simulation is performed in a finite domain, and Laitone's formulae are valid for an indefinitely long channel, care must be taken choosing the initial position of the wave crest. In order to deal with it, the use of the effective wave length  $\lambda$  concept is made.  $\lambda$  is equal to the doubled length between the wave crest and a point, where the free surface elevation is  $\eta(x) = 0.01H$ . According to Laitone:

$$\lambda = 6.9 \sqrt{\frac{h^3}{H}} \quad (21.2)$$

For example, when  $H/h = 0.1$ ,  $\lambda/2 \approx 11h$ , and for a channel of 10m depth, the initial distance between the solitary wave crest and a boundary should be at least 110m.

## 21.4 Description

### 21.4.1 Geometry and Mesh

#### Geometry

A long channel of 600m long and 6m wide is considered, with a constant depth  $h = 10m$ . The bottom is flat, at the elevation  $z = -10m$ .

## Mesh

The mesh is composed of 6 elements on the width and 600 on the length, with a resolution in the direction parallel to the channel axis of 1m (see the Figure 21.2). This corresponds to 7,206 triangular elements and 4,210 nodes. Various numbers of planes on the vertical are considered: 2, 3 and 4.

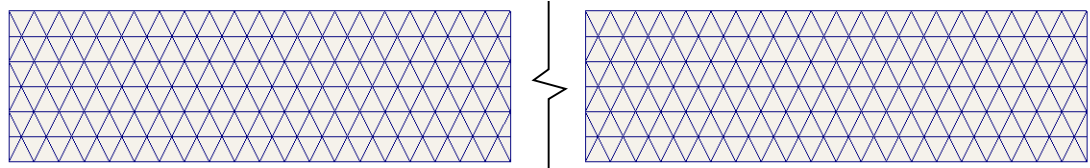


Figure 21.2: Solitary wave propagation over a flat bottom: mesh of the case in the  $(x,y)$  plane.

### 21.4.2 Physical parameters

The flow is assumed to be inviscid, without shear on the lateral boundaries and on the bottom.

### 21.4.3 Initial and Boundary Conditions

#### Initial conditions

As the initial condition the hydrostatic approximation given by (21.1) is applied, with a wave height of  $H = 1m$ , and the initial crest position at  $x = 150m$ . The velocity field and the free-surface elevation are given by (21.1).

#### Boundary conditions

The lateral boundaries and the bottom are impervious, there is no friction.

### 21.4.4 General parameters

The time step size is constant, equal to  $\Delta t = 0.1s$  (the Courant number in the direction of wave propagation varies from 0.2 to about 1.0 at the wave crest). The simulation time is 30s.

### 21.4.5 Numerical parameters

The non-hydrostatic version is used. Advection of velocities is done with the method of characteristics. The solver for the pressure is a conjugate gradient with diagonal preconditionning, an accuracy of  $1e - 6$  is asked for with a maximum number of iterations of 500. A coefficient of implicitation for the depth and velocities of 0.51 is used. A mass-lumping is used on the depth, with a coefficient of 1. There are no tidal flats in this case.

## 21.5 Results

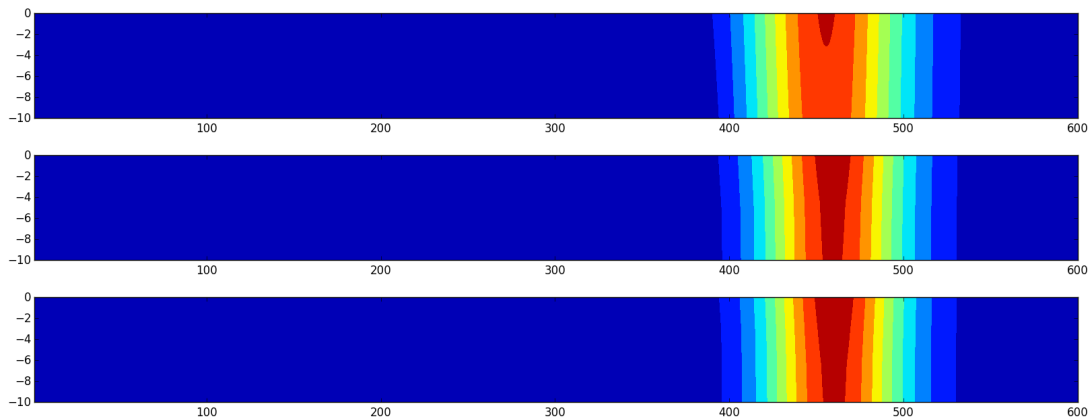


Figure 21.3: Solitary wave propagation over a flat bottom: simulation results using 2, 3 and 4 planes: the colours represent the velocity magnitude, from 0 (blue) to 1 (red).

Figure 21.3 presents a longitudinal cross profile of the free surface at different times of the simulation and for the various configurations on vertical discretisation. The amplitude of the wave remains nearly constant in all cases. The relative error on the wave amplitude after 30s is of 4.8% with 2 planes and about 0.01% with 3 and 4 planes (see the Table 21.1). On the other hand, the theoretical celerity of the propagation is equal to  $\sqrt{g(h+H)}$ . With a water level  $h = 10m$  and a wave height  $H = 1m$ , the theoretical celerity is equal to  $10.38ms^{-1}$ . Table 21.1 shows the values of the wave displacement and celerity on the numerical models (using 2, 3 and 4 planes). The error on the celerity is also displayed, showing a maximum error of 1.9% (using two planes) and less than 1% when refining on the vertical.

Table 21.1: Solitary wave propagation over a flat bottom: values of the wave height and displacement after 30s in the simulation, together with the values of wave celerity and relative error on the celerity using 2, 3 and 4 planes in the mesh.

	<b>2 planes</b>	<b>3 planes</b>	<b>4 planes</b>
<b>Final wave height (m)</b>	0.952	0.999875	1.0002
<b>Final displacement (m)</b>	305.5	309	310
<b>Wave celerity (<math>ms^{-1}</math>)</b>	10.18	10.3	10.33
<b>Relative error on the celerity (%)</b>	1.9	0.8	0.5

### Results using the hydrostatic version of TELEMAC-3D

The users should be aware that when using the hydrostatic version on this test-case, the results are not in good agreement with the approximate theoretical solution: the shape of the velocity field is deteriorated, the error on the wave celerity is of about 10% and the error on the wave height after 30s of propagation is of 15%.

## 21.6 Conclusion

TELEMAC-3D correctly simulates the propagation of a solitary wave when using the non-hydrostatic formulation.

## 22. source

### 22.1 Purpose

This test shows the capability of TELEMAC-3D to manage multiple sources of fluid and tracers. It also demonstrates the ability to compute injection and conservation of multiple tracers.

### 22.2 Description

We consider a basin at rest. Sources are specified at some points of the mesh. 3 tracers are used, one is the sum of the 2 others.

#### 22.2.1 Reference

#### 22.2.2 Geometry and Mesh

##### Bathymetry

Flat bottom ( $z = -1$  m)

Constant water depth = 1 m

##### Geometry

Basin length = 100 m

Basin width = 40 m (figure 22.1)

##### Mesh

674 triangular elements

373 nodes

5 layers regularly spaced on the vertical

#### 22.2.3 Physical parameters

Constant vertical and horizontal viscosities:  $10^{-6}$  m<sup>2</sup>/s

Coriolis: no

Wind: no

#### 22.2.4 Initial and Boundary Conditions

##### Initial conditions

No velocity

Null water level

No tracers

### Boundary conditions

Channel banks: solid boundary without roughness  
Bottom: solid boundary roughness

### 22.2.5 General parameters

Time step: 1.1 s  
Simulation duration: 1,100 s

### 22.2.6 Numerical parameters

Hydrostatic simulation  
Advection of velocities: characteristics  
Advection of tracers: edge by edge explicit finite volume Leo Postma scheme for tidal flats

### 22.2.7 Definition of sources

Position source 1:  $x \approx -21.6$  m,  $y \approx 5.3$  m,  $z = -0.5$  m  
Position source 2:  $x \approx -0.8$  m,  $y \approx -10.$  m,  $z = -0.5$  m  
Constant discharge of 1 m<sup>3</sup>/s at both sources  
Tracer concentration at sources: 10 g/L (or kg/m<sup>3</sup>)  
Source 1 discharges tracer 1 and 2  
Source 2 discharges tracer 2 and 3  
Source 2 has an initial velocity:  $U = 0.5$  m/s,  $V = 2$  m/s  
The definition of the discharges and tracer concentrations at sources has been done in the SOURCES FILE. As this last file is present in the examples directory, the keyword VALUES OF THE TRACERS AT THE SOURCES is ignored but is given as an example coherent with what is done in the SOURCES FILE.

### 22.2.8 Comments

## 22.3 Results

Figure 22.1 shows the horizontal mesh and sources positions in the upper panel.

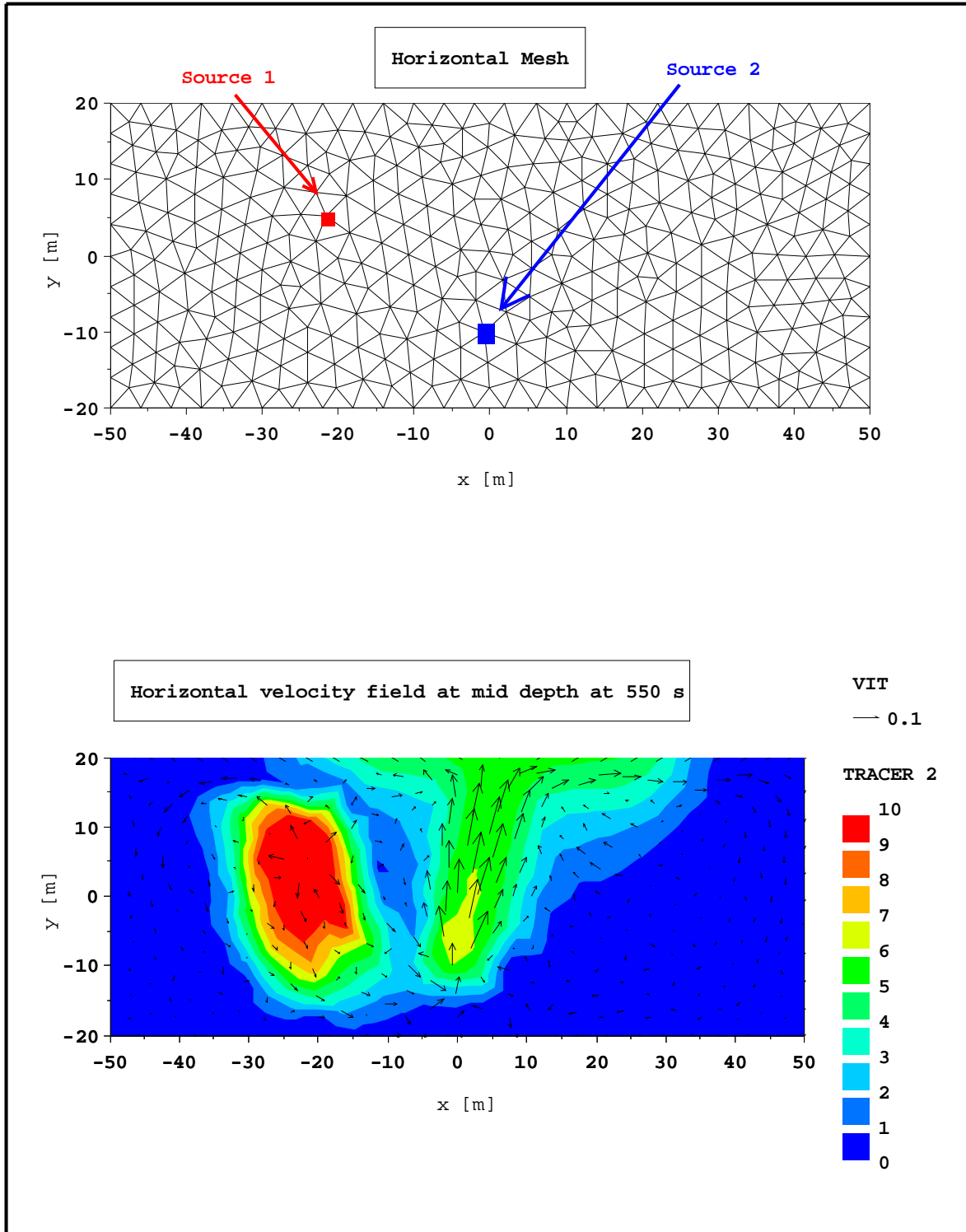


Figure 22.1: Source test: Mesh and horizontal velocity field

The lower panel highlights the influence of the initial velocity of source 2 on the horizontal velocity field at mid depth at 550 s. Additionally, the lower panel shows tracer 2 spreads in every direction at source 1, unlike at source 2 where tracer 2 diffuses in the initial velocity direction.

The horizontal and vertical plumes of each tracer at 1,100 s, on figures 22.2 and 22.3 respec-

tively, allows verifying that the plume of tracer 2 is the combination of the plumes of tracer 1 and 3.

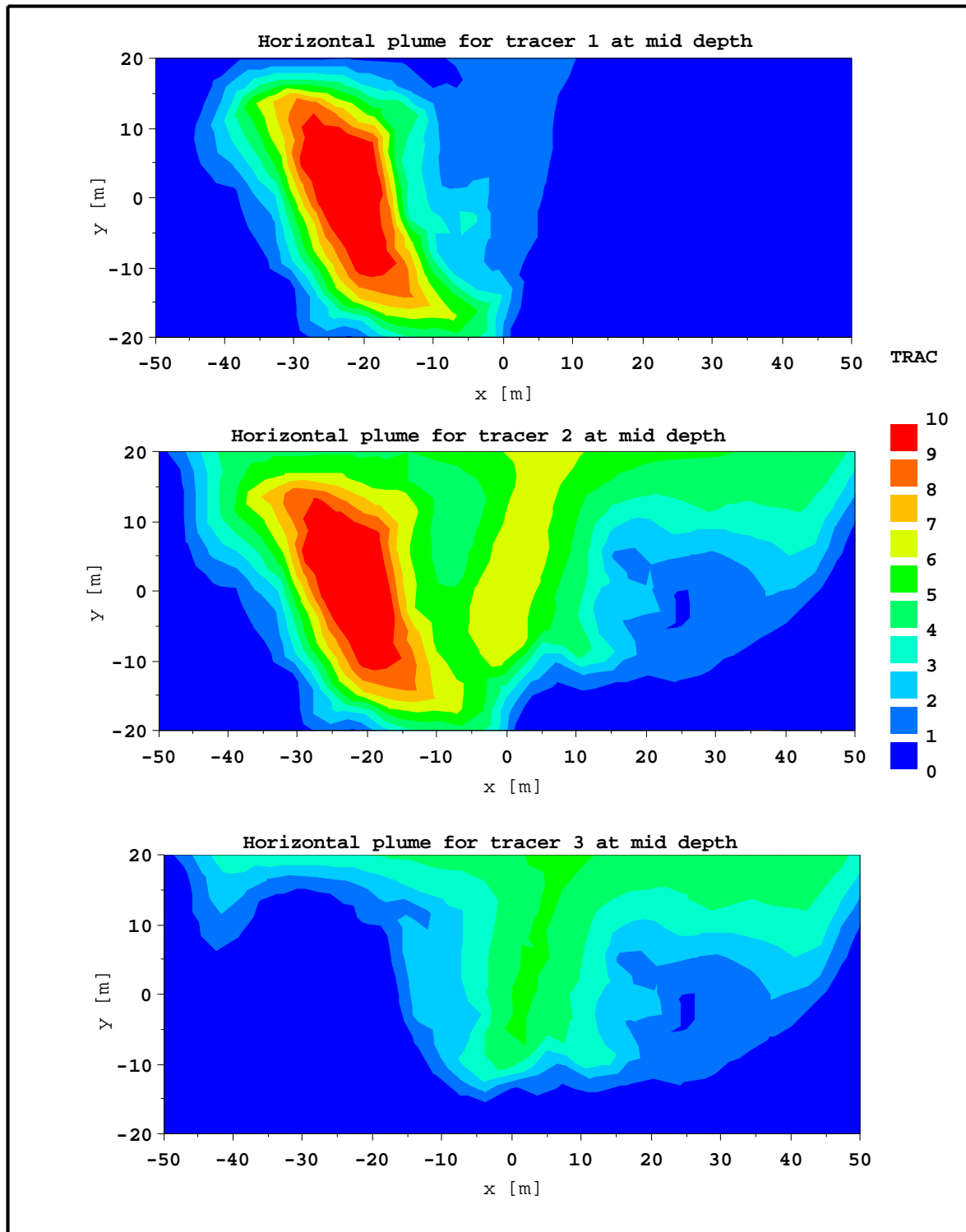


Figure 22.2: Source test: Horizontal shape of the plumes

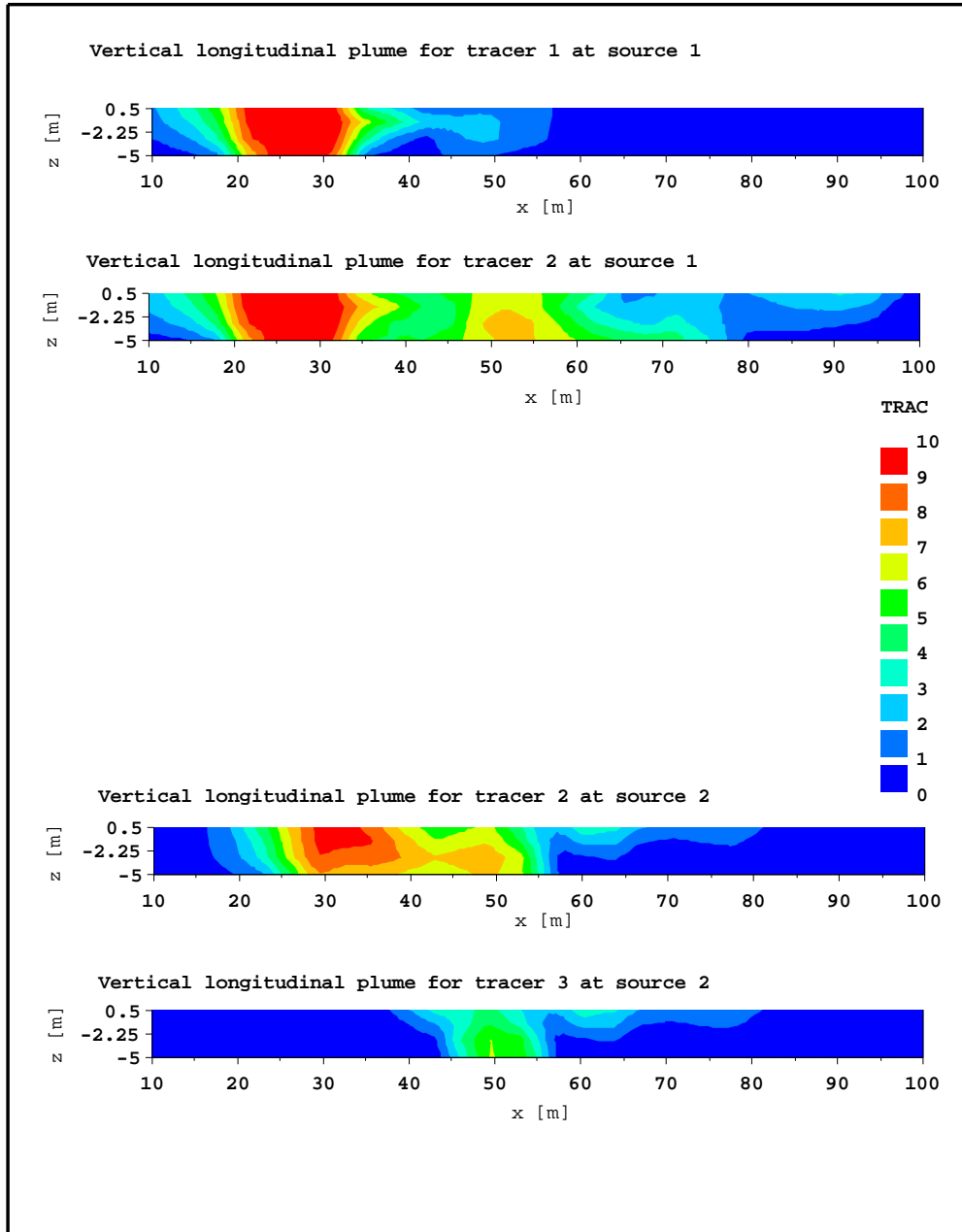


Figure 22.3: Source test: Vertical shape of the plumes

Moreover, the following mass balance of the TELEMAC-3D simulation shows that the amount of water injected by the sources is very good ( $2,200 \text{ m}^3 = 2 \text{ sources} \times 1 \text{ m}^3/\text{s} \times 1,100 \text{ s}$  with an error lower than  $10^{-6} \text{ m}^3$ , thus a relative error lower than  $10^{-9}$ ). If the keywords for accuracy for propagation and diffusion of tracers are equal to  $10^{-14}$ , the error becomes lower than  $10^{-12} \text{ m}^3$ , thus a relative error lower than the machine accuracy  $10^{-15}$ ). The mass balance also shows the conservation and the amount of discharged tracer 1, 2 and 3 is good (e.g. for tracer 2:  $10 \text{ kg/m}^3 \times 2 \text{ sources} \times 1,100 \text{ s} \times 1 \text{ m}^3/\text{s} = 22,000 \text{ kg}$  with an error lower than  $10^{-5} \text{ kg}$ , so a relative error lower than  $10^{-9}$ ). To get an error lower than  $2.10^{-8} \text{ kg}$ , so a relative error lower than  $2.10^{-12}$ , an accuracy of  $10^{-14}$  is required for the diffusion of tracers and propagation. Otherwise, the mass balances may be worse but sufficient enough, depending on the accuracy the user wishes.

Balance for ACCURACY FOR PROPAGATION =  $10^{-8}$  and ACCURACY FOR DIFFUSION

OF TRACERS =  $10^{-9}$  in serial:

```

FINAL MASS BALANCE
T = 1100.0000

--- WATER ---
INITIAL MASS : 4000.000
FINAL MASS : 6200.000
MASS LEAVING THE DOMAIN (OR SOURCE) : -2200.000
MASS LOSS : 0.2391803E-06

--- TRACER 1: TRACER 1 , UNIT : ?? * M3)
INITIAL MASS : 0.000000
FINAL MASS : 11000.00
MASS EXITING (BOUNDARIES OR SOURCE) : -11000.00
MASS LOSS : 0.5897147E-05

--- TRACER 2: TRACER 2 , UNIT : ?? * M3)
INITIAL MASS : 0.000000
FINAL MASS : 22000.00
MASS EXITING (BOUNDARIES OR SOURCE) : -22000.00
MASS LOSS : 0.2584195E-05

--- TRACER 3: TRACER 3 , UNIT : ?? * M3)
INITIAL MASS : 0.000000
FINAL MASS : 11000.00
MASS EXITING (BOUNDARIES OR SOURCE) : -11000.00
MASS LOSS : -0.3261903E-05

```

Balance for ACCURACY FOR PROPAGATION =  $10^{-8}$  and ACCURACY FOR DIFFUSION OF TRACERS =  $10^{-9}$  in parallel (4 processors):

```

FINAL MASS BALANCE
T = 1100.0000

--- WATER ---
INITIAL MASS : 4000.000
FINAL MASS : 6200.000
MASS LEAVING THE DOMAIN (OR SOURCE) : -2200.000
MASS LOSS : 0.2392089E-06

--- TRACER 1: TRACER 1 , UNIT : ?? * M3)
INITIAL MASS : 0.000000
FINAL MASS : 11000.00
MASS EXITING (BOUNDARIES OR SOURCE) : -11000.00
MASS LOSS : 0.5897227E-05

--- TRACER 2: TRACER 2 , UNIT : ?? * M3)
INITIAL MASS : 0.000000
FINAL MASS : 22000.00
MASS EXITING (BOUNDARIES OR SOURCE) : -22000.00
MASS LOSS : 0.2584398E-05

--- TRACER 3: TRACER 3 , UNIT : ?? * M3)
INITIAL MASS : 0.000000
FINAL MASS : 11000.00
MASS EXITING (BOUNDARIES OR SOURCE) : -11000.00
MASS LOSS : -0.3261772E-05

```

Balance for ACCURACY FOR PROPAGATION =  $10^{-14}$  and ACCURACY FOR DIFFUSION OF TRACERS =  $10^{-14}$  in serial:

```

FINAL MASS BALANCE
T = 1100.0000

--- WATER ---
INITIAL MASS : 4000.000
FINAL MASS : 6200.000
MASS LEAVING THE DOMAIN (OR SOURCE) : -2200.000
MASS LOSS : 0.4547474E-12

--- TRACER 1: TRACER 1 , UNIT : ?? * M3)
INITIAL MASS : 0.000000
FINAL MASS : 11000.00
MASS EXITING (BOUNDARIES OR SOURCE) : -11000.00
MASS LOSS : -0.1768058E-07

--- TRACER 2: TRACER 2 , UNIT : ?? * M3)
INITIAL MASS : 0.000000
FINAL MASS : 22000.00
MASS EXITING (BOUNDARIES OR SOURCE) : -22000.00
MASS LOSS : -0.1020817E-07

--- TRACER 3: TRACER 3 , UNIT : ?? * M3)
INITIAL MASS : 0.000000
FINAL MASS : 11000.00
MASS EXITING (BOUNDARIES OR SOURCE) : -11000.00
MASS LOSS : 0.7525159E-08

```

## 22.4 Conclusion

TELEMAC-3D is able to compute the evolution and conservation of tracers discharged by sources.

# 23. stratification

## 23.1 Purpose

This test demonstrates the ability of TELEMAC-3D to model stratified flow with a special focus on the stability of the stratification. This case also demonstrates the capacity of the  $k-\varepsilon$  model to generate turbulent phenomenon.

## 23.2 Description

We consider a channel 2,000 m long and 100 m wide. The bottom of this channel has a very mild slope. The general water depth is 10 m and the velocity along the channel is constant and equal to 1 m/s. Salinity is prescribed as shown on figure 3.10.2.

### 23.2.1 Reference

### 23.2.2 Geometry and Mesh

#### Bathymetry

Mild slope bottom (0 at the entrance, -1.9 cm at the output)

#### Geometry

Channel length = 2,000 m

Channel width = 100 m (see figure 3.10.1)

#### Mesh

2,204 triangular elements

1,188 nodes

21 planes regularly spaced on the vertical

### 23.2.3 Physical parameters

Horizontal and vertical turbulence models:  $k-\varepsilon$  model

Bottom friction: Strickler coefficient =  $70 \text{ m}^{1/3}/\text{s}$

Coriolis: no

Wind: no

### 23.2.4 Initial and Boundary Conditions

#### Initial conditions

Constant longitudinal velocity = 1 m/s

Constant water depth = 10 m

Constant tracer = 38 at the bottom below the plane number 18 and 28 at the top above the plane number 18

#### Boundary conditions

Upstream: prescribed flow rate and tracer.

Downstream: prescribed water depth

Bottom: solid boundary with roughness

Lateral wall: no friction

### 23.2.5 General parameters

Time step: 2 s

Simulation duration 2,000 s

### 23.2.6 Numerical parameters

Advection of velocities, tracer and  $k$ - $\varepsilon$ : N-type MURD scheme

### 23.2.7 Comments

The tracer and velocity field are directly included in the CONDIM subroutine.

## 23.3 Results

The vertical gradient of salinity remains stable as shown on figure 3.10.2. On figure 3.10.3, we can observe the generation of the turbulence phenomenon by the  $k$ - $\varepsilon$  model. This turbulence is created at the bottom and is developing on the vertical column of water. However, the turbulence is clearly blocked by the saline stratification.

## 23.4 Conclusion

TELEMAC-3D is able to represent correctly stratified flow. In addition, the  $k$ - $\varepsilon$  model is able to simulate turbulence generated by bottom friction.

# 24. tetra

## 24.1 Purpose

This test demonstrates the ability of TELEMAC-3D to be discretised with prisms split into tetrahedra.

To compare the solution produced by TELEMAC-3D in a frictionless channel presenting an idealised bump on the bottom with the analytical solution to this problem.

The flow regime is sub-critical.

The channel is horizontal with a 4 m long bump in its middle. The maximum elevation of the bump is 20 cm.

The tracer used is salinity.

## 24.2 Description

### 24.2.1 Reference

### 24.2.2 Geometry and Mesh

#### Bathymetry

If  $6.51 \text{ m} < x < 13.49 \text{ m}$ ,  $z_f = -0.0246875(x - 10)^2$

If  $x < 1.44 \text{ m}$ ,  $z_f = -0.2 - 0.3(\frac{x}{2.5})^2$

$z_f = -0.3 \text{ m}$  elsewhere

#### Geometry

It is the same geometry as the TELEMAC-2D test case “bumflu”.

#### Mesh

2,620 triangular elements

1,452 nodes

10 planes regularly spaced in the vertical direction except one fixed plane with the elevation -0.2 m (plane number 4).

### 24.2.3 Physical parameters

Turbulence model:  $k - \varepsilon$  model

Coriolis: no

**24.2.4 Initial and Boundary Conditions****Initial conditions**

Constant initial water level at  $z = 1.8$  m

No velocity

Initial tracer: uniform 30

**Boundary conditions**

Upstream: imposed flow rate ( $4 \text{ m}^3/\text{s}$ ) and imposed tracer ( $40$  if  $z \leq -0.2 \text{ m}$ ,  $30$  if  $z > -0.2 \text{ m}$ )

Downstream: prescribed elevation  $1.8$  m so that the water depth is  $2$  m

**24.2.5 General parameters**

Time step:  $0.04$  s

Simulation duration:  $40$  s

**24.2.6 Numerical parameters**

Non-hydrostatic version

Advection for velocities: edge by edge explicit finite volume Leo Postma

Advection for tracers: edge by edge explicit finite volume Leo Postma

Advection for  $k - \varepsilon$ : edge by edge explicit finite volume Leo Postma

**24.2.7 Comments****24.3 Results****24.4 Conclusion**

# 25. thomson

## 25.1 Purpose

This test is identical to case 3.3 but with open boundaries. It shows that the circular wave propagates out of the computational domain freely without any reflexion. It demonstrates that the TELEMAC-3D solution is not polarised because it can simulate the circular spreading of a wave in square computation domain. Moreover, it also demonstrates that TELEMAC-3D is capable to deal with open boundaries without prescribing water depth or velocity by using the Thompson method based on characteristic.

## 25.2 Description

The fluid is initially at rest with a Gaussian free surface in the centre of a square domain (see figure 3.14.2).

The evolution of the surface is then calculated during 4 seconds.

### 25.2.1 Reference

### 25.2.2 Geometry and Mesh

#### Bathymetry

Flat bottom

#### Geometry

Square length = 20.1 m

#### Mesh

8,978 triangular elements

4,624 nodes

3 planes regularly spaced on the vertical (see figure 3.14.1)

### 25.2.3 Physical parameters

Turbulence: constant viscosity in both directions (molecular viscosity)

Bottom friction: Chézy law with coefficient equal to  $60 \text{ m}^{1/2}/\text{s}$

Coriolis: no

Wind: no

#### 25.2.4 Initial and Boundary Conditions

##### Initial conditions

Water depth at boundary: 2.4 m

Water depth at the centre: 4.8 m

No velocity

##### Boundary conditions

Open boundary with the Thompson method based on characteristic

#### 25.2.5 General parameters

Time step: 0.04 s

Simulation duration: 4 s

#### 25.2.6 Numerical parameters

Non-hydrostatic computation

Advection for velocities: PSI-type MURD scheme

Free surface gradient compatibility coefficient: 0.

#### 25.2.7 Comments

The initial free surface elevation is prescribed in the CONDIM subroutine

### 25.3 Results

Figures 3.14.3 to 3.14.5 show that the wave spreads circularly around the initial water surface peak elevation when it reaches the boundaries, the wave goes out of the domain freely, no reflection occurs.

### 25.4 Conclusion

Even though the mesh is polarised (along the  $x$  and  $y$  directions and the main diagonal), the solution is not.

Open boundaries are treated properly: no bias occurs. Moreover, using the Thompson methods method based on characteristic enable to use open boundaries (444) without the need to specify water depth or velocity at the boundary.

# 26. tide

## 26.1 Purpose

This test demonstrates the availability of TELEMAC-3D to model the propagation of tide in a maritime domain by computing tidal boundary conditions.

## 26.2 Description

A coastal area located in the English Channel off the coast of Brittany (in France) close to the real location of the Paimpol-Bréhat tidal farm is modelled to simulate the tide and the tidal currents over this area. Time and space varying boundary conditions are prescribed over liquid boundaries.

### 26.2.1 Reference

### 26.2.2 Geometry and Mesh

#### Bathymetry

Real bathymetry of the area bought from the SHOM (French Navy Hydrographic and Oceanographic Service). ©Copyright 2007 SHOM. Produced with the permission of SHOM. Contract number 67/2007

#### Geometry

Almost a rectangle with the French coasts on one side  $22\text{ km} \times 24\text{ km}$

#### Mesh

4,385 triangular elements

2,386 nodes

11 planes regularly spaced on the vertical

### 26.2.3 Physical parameters

Vertical turbulence model: mixing length model

Horizontal viscosity for velocity:  $10^{-4}\text{ m}^2/\text{s}$

Coriolis: yes (constant coefficient over the domain =  $1.10 \times 10^{-4}\text{ rad/s}$ )

No wind, no atmospheric pressure, no surge and nor waves

#### **26.2.4 Initial and Boundary Conditions**

##### **Initial conditions**

Constant elevation

No velocity

##### **Boundary conditions**

Elevation and horizontal velocity boundary conditions computed by TELEMAC-3D from an harmonic constants database (JMJ from LNH).

#### **26.2.5 General parameters**

Time step: 20 s

Simulation duration: 90,000 s = 25 h

#### **26.2.6 Numerical parameters**

Non-hydrostatic version

Advection for velocities: Characteristics method

Thompson method with calculation of characteristics for open boundary conditions

Free Surface Gradient Compatibility = 0.5 (not 0.9) to prevent on wiggles

Tidal flats with correction of Free Surface by elements, treatments to have  $h \geq 0$

#### **26.2.7 Comments**

#### **26.3 Results**

Tidal range, sea levels and tidal velocities are well reproduced compared to data coming from the SHOM or at sea measurements.

#### **26.4 Conclusion**

TELEMAC-3D is able to model tide in coastal areas.

# 27. uneven

## 27.1 Purpose

This test demonstrates the availability of TELEMAC-3D to propagate a wave over an uneven seabed.

## 27.2 Description

A rectangular channel is considered.

A solitary wave propagates over an uneven seabed.

### 27.2.1 Reference

### 27.2.2 Geometry and Mesh

#### Bathymetry

A piecewise affine bathymetry only dependent on the abscissa coordinate  $x$  is defined.

#### Geometry

Channel length = 600 m

Channel width = 6 m

#### Mesh

7,206 triangular elements

4,210 nodes

3 planes regularly spaced on the vertical

### 27.2.3 Physical parameters

No diffusion

Coriolis: no

### 27.2.4 Initial and Boundary Conditions

#### Initial conditions

Solitary wave initial velocity (analytical solution) for the water depth and the horizontal velocity components

#### Boundary conditions

Closed boundaries. No bottom friction

**27.2.5 General parameters**

Time step: 0.25 s

Simulation duration: 25 s

**27.2.6 Numerical parameters**

Non-hydrostatic version

Advection for velocities: Characteristics method

**27.2.7 Comments****27.3 Results****27.4 Conclusion**

# 28. vasque

## 28.1 Purpose

This test demonstrates the ability of TELEMAC-3D to model water retention in a bowled beach during ebbing tide.

## 28.2 Description

We consider a beach profile presenting a bowl. The water level is initially at high tide level. We simulate the ebbing tide with the seaward final water level below the beach bowl.

### 28.2.1 Reference

### 28.2.2 Geometry and Mesh

#### Bathymetry

The bathymetry is a beach profile starting at  $z = -0.14$  m, presenting a bowl, and ending at  $z = -0.6$  m (see figure 3.16.1)

#### Geometry

Beach length = 46 m

Beach width = 9 m

#### Mesh

828 triangular elements

470 nodes

10 planes regularly spaced on the vertical (see figure 3.16.1)

### 28.2.3 Physical parameters

Turbulence: constant viscosity in both directions of  $0.1 \text{ m}^2/\text{s}$

Bottom friction: Strickler law with coefficient equal to  $40 \text{ m}^{1/3}/\text{s}$

Coriolis: no

Wind: no

### 28.2.4 Initial and Boundary Conditions

#### Initial conditions

Constant free surface level at  $z = 0$  m (high tide)

No velocity

**Boundary conditions**

Closed boundaries on sides and landward

Seaward boundary controlling decreasing water depth (ebbing tide) with SL3 function

**28.2.5 General parameters**

Time step: 0.5 s

Simulation duration: 300 s

**28.2.6 Numerical parameters**

Non-hydrostatic computation

Advection for velocities: Characteristics

**28.2.7 Comments**

The bowed beach profile is specified in the T3D\_CORFON subroutine.

**28.3 Results**

Figure 3.16.2 presents longitudinal cross profiles of water level at initial and final times of the simulation. At final time, the bowl is filled of water while the seaward water level is below the bowl position.

**28.4 Conclusion**

TELEMAC-3D is capable to model water retention in bathymetry bowls.

## 29. vent

### 29.1 Purpose

This test demonstrates the availability of TELEMAC-3D to represent the currents induced by wind blowing at the surface of a closed channel. More precisely, this case allows verifying that a linear decrease of the mixing length model at the bottom and at the surface is able to reproduce such circulation. Moreover, this test allows verifying the proper implementation of the sources terms and external forces as the wind.

### 29.2 Description

At the initial state, the channel is submitted to a constant 10 m/s wind. The wind generates a slope of the free surface and a vertical two-dimensional circulation. Tsanis [1] has made an inventory of existing laboratory or in-situ measurements and has plotted these values on a non-dimensional graph. He deduced a characteristic vertical velocity profile, which will be compared to the numerical results of this test case. The turbulent viscosity has the following expression:

$$v_t = l^2 \sqrt{\frac{1}{2} \left[ \frac{\partial u_i}{\partial x_j} + \frac{\partial u_j}{\partial x_i} \right]^2} \quad (29.1)$$

$l$  = mixing length

$K$  = 0.40 Karman constant

The channel is a rectangle of 500 m by 100 m with horizontal bed at depth  $z = -10$  m.

With:

$$\mathbf{w} = 10 \text{ m/s Velocity of wind} \quad (29.2)$$

$$K_F = (-0.12 + 0.137 \|\mathbf{w}\|)/1000 \quad (29.3)$$

#### 29.2.1 Reference

[1] TSANIS I., Simulation of wind-induced water currents, Journal of Hydraulic Engineering, Vol.115, n 8, 1989, pp 1113-1134.

[2] WU J., Prediction of near-surface drift currents from wind velocity, Journal of Hydraulic Division, 99, 1973, pp 1291-1302.

## 29.2.2 Geometry and Mesh

### Bathymetry

Constant equal to  $-10\text{ m}$

### Geometry

Channel length =  $500\text{ m}$

Channel width =  $100\text{ m}$

### Mesh

543 triangular elements

315 nodes

15 planes irregularly spaced on the vertical (see figure 3.4.1 generated with a vertical expansion factor equal to 20)

## 29.2.3 Physical parameters

Vertical turbulence model: Tsanis mixing length turbulence model

Horizontal viscosity for velocity:  $0.1\text{ m}^2/\text{s}$

Coriolis: no

Wind:  $10\text{ m/s}$  in  $x$  direction

## 29.2.4 Initial and Boundary Conditions

### Initial conditions

No velocity, initial water level equal to zero

### Boundary conditions

Channel banks: solid slip boundary

Bottom: solid boundaries with friction stress due to mixing length

Surface: shear stress wind

## 29.2.5 General parameters

Time step:  $10\text{ s}$

Simulation duration:  $20,000\text{ s}$  ( $5\text{ h }33\text{ min }20\text{ s}$ )

## 29.2.6 Numerical parameters

Hydrostatic computation

Advection for velocities: PSI-type MURD scheme

Diagonal preconditioning for propagation

## 29.2.7 Comments

### 29.3 Results

The mass balance is the following:

MASSE INITIALE (DEBUT DE CE CALCUL) :	500000.0
MASSE FINALE :	500000.0
MASSE SORTIE DU DOMAINE (OU SOURCE) :	0.000000
MASSE PERDUE :	-0.5280007E-03

Thus, the mass balance is consistent with the accuracy asked (from  $10^{-8}$  to  $10^{-6}$  depending on the system to solve, for the diffusion of velocities, propagation or vertical velocity). Figure 3.4.2 shows the vertical circulation induced by the wind. The velocity at the surface is  $18\text{ cm/s}$

and the return current reaches a maximum value of 5.7 cm/s. However, it must be pointed out that the velocity at the surface depends on the refinement near the surface because the velocity gradient is very high in this area. A distance between the two first vertical points of 0.50 m instead of 0.10 m induced a velocity at the surface of 12 cm/s, but the velocity field below 1 m under the surface was only slightly modified. J. Wu [2] proposed for the velocity  $u_s$  at the surface the expression:

$$u_s = 0.55(\tau/\rho_{air})^{1/2} \quad (29.4)$$

. This gives  $u_s = 19$  cm/s. Then, the velocity computed with a mesh of 0.10 m is very close to this theoretical value. Figure 3.4.2 shows the non-dimensional plot of the vertical velocity profile. The numerical results fit the measurements reasonably well. The upper part of the profile, where the velocities have the same orientation as the wind, is close to measured profiles, but the lower part is smoothed. This could mean that the level of turbulence is stronger in nature. The slope of the free surface presented in figure 3.4.3 is equal to  $1.576 \cdot 10^{-6}$ . The computation of the slope, assuming that the flow is homogeneous on the vertical, gives a slope equals to  $1.66 \cdot 10^{-6}$ . This value is in agreement with the value given by TELEMAC-3D.

## 29.4 Conclusion

The velocity field produced by TELEMAC-3D using the standard mixing length is correct. Near the surface, the quality of the results depends on the vertical resolution near the surface. The second points of the vertical mesh should be 10 cm below the surface for a good result. In the deeper part, the profile is a little bit more smoothed. Taking into account the effect of the wind directly into the turbulence model may ameliorate this result.

- [1] C. Adduce, G. Sciortino, and S. Proietti. Gravity currents produced by lock exchanges: Experiments and simulations with a two-layer shallow-water model with entrainment. *Journal of Hydraulic Research*, 138(2), 2012.
- [2] D. Barr. Densimetric exchange flow in rectangular channels. III. large scale experiments. *La Houille Blanche*, (22):619–632, 1967.
- [3] T. Benjamin. Gravity currents and related phenomena. *Journal of Fluid Mechanics*, 31(2): 209–248, 1968.
- [4] J.A. Jankowski. *A non-hydrostatic model for free surface flows*. PhD thesis, Universität Hannover, 1999. Bericht Nr. 56/1999, Institut für Strömungsmechanik und ERIB.
- [5] E. V. Laitone. The second approximation to cnoidal and solitary waves. *Journal of Fluid Mechanics*, 9:430–444, 1960.
- [6] B. Ramaswamy. Numerical simulation of unsteady viscous free surface flow. *Journal of Computational Physics*, 90:396–430, 1990.